UNIVERSITY OF Nebraska Lincoln

THE UNIVERSITY OF IOWA

KU THE UNIVERSITY OF KANSAS

MISSOURI S&T

LINCOLN UNIVERSITY MISSOURI

NICC NEBRASKA INDIAN COMMUNITY COLLEGE

UNIVERSITY OF Nebraska Omaha

University of Nebraska Medical Center

KU MEDICAL CENTER The University of Kansas

Performance of Earthquake-Damaged Reinforced Concrete Bridges with Repaired Columns - Phase II

Lesley H. Sneed, PhD, PE, SE
Professor
Department of Civil, Materials, and Environmental Engineering
University of Illinois at Chicago
Adjunct Professor
Department of Civil, Architectural, and Environmental Engineering
Missouri University of Science and Technology

Giacomo Fraioli
Graduate Research Assistant
Department of Civil, Architectural, and Environmental Engineering
Missouri University of Science and Technology

MISSOURI S&T

2021

MATC

Performance of Earthquake-Damaged Reinforced Concrete Bridges with Repaired Columns - Phase II

Giacomo Fraioli
Graduate Research Assistant
Department of Civil, Architectural and Environmental Engineering
Missouri University of Science and Technology, Rolla, MO

Lesley H. Sneed, Ph.D., P.E., S.E.
Professor
Department of Civil, Materials and Environmental Engineering
University of Illinois at Chicago, Chicago, IL
Adjunct Professor
Department of Civil, Architectural and Environmental Engineering
Missouri University of Science and Technology, Rolla, MO

A Report on Research Sponsored by

Mid-America Transportation Center

University of Nebraska–Lincoln

December 2021

Technical Report Documentation Page

1. Report No. 25-1121-0005-136-3	2. Government Accession No.	3. Recipient's Catalog No.
4. Title and Subtitle Performance of Earthquake-Damaged Reinforced Concrete Bridges with Repaired Columns - Phase II	5. Report Date December 2021	
	6. Performing Organization Code	
7. Author(s) Giacomo Fraioli, http://orcid.org/0000-0003-3054-2903, Lesley H. Sneed, Ph.D, http://orcid.org/0000-0003-1528-5611	8. Performing Organization Report No. 25-1121-0005-136-3	
9. Performing Organization Name and Address Missouri University of Science and Technology, Rolla, MO	10. Work Unit No. (TRAIS)	
	11. Contract or Grant No. 69A3551747107	
12. Sponsoring Agency Name and Address Mid-America Transportation Center 2200 Vine St. PO Box 830851 Lincoln, NE 68583-0851	13. Type of Report and Period Covered Final Report Jan 2020 – Dec 2021	
	14. Sponsoring Agency Code MATC TRB RiP No. 91994-54	
15. Supplementary Notes Conducted in cooperation with the U.S. Department of Transportation, Federal Highway Administration.		

16. Abstract

This report summarizes the second phase of an investigation on the performance of earthquake-damaged reinforced concrete bridges with repaired columns. In Phase II, a study was conducted to optimize the level of (pre-earthquake) retrofit of RC bridge columns that can be rapidly repaired (i.e., in a 3-day period) in the event of an earthquake. Retrofit and repair of earthquake-damaged reinforced concrete (RC) bridge columns have been studied extensively in the past several years; however, no studies have been conducted on the optimization process on the combined levels of retrofit and rapid repair. In this study, a framework is presented to optimize the combined levels of retrofit and rapid repair needed to maintain the level of serviceability of a bridge effected by an earthquake. Numerical simulation was used to model the response of two RC bridge columns with different reinforcement details and retrofitted with different methods that were reported in the literature. Incremental dynamic analysis (IDA) was used to determine the seismic response of a prototype bridge system that included the retrofitted RC columns to determine how different methods and levels of column retrofit affect the system-level response of the bridge structure and its ability to be repaired after an earthquake. Knowledge of the system-level performance can, in turn, be used to manage the levels of retrofit and repair to help ensure the survival of the infrastructure while reducing initial costs.

17. Key Words Columns, Reinforced Concrete Bridges, Earthquake damage, Incremental Dynamic Analysis, Repairing, Retrofitting		18. Distribution Statement No restrictions.		
19. Security Classif. (of this report) Unclassified		20. Security Classif. (of this page) Unclassified	21. No. of Pages 55	22. Price

Table of Contents

List of Figures

List of Tables

List of Abbreviations

Cast in place (CIP)
Damage measure (DM)
Damage state (DS)
Drift limit (DL)
Externally bonded (EB)
Federal Highway Administration (FHWA)
Fiber reinforced polymer (FRP)
Glass fiber reinforced polymer (GFRP)
Ground motion (GM)
Incremental dynamic analysis (IDA)
Intensity measure (IM)
Mid-America Transportation Center (MATC)
Missouri University of Science & Technology (Missouri S&T)
Open System for Earthquake Engineering Simulation (OpenSees)
Pacific Earthquake Engineering Research (PEER)
Peak ground acceleration (PGA)
Reinforced concrete (RC)
United States Geological Survey (USGS)

Acknowledgments

Disclaimer

The contents of this report reflect the views of the authors, who are responsible for the facts and the accuracy of the information presented herein. This document is disseminated in the interest of information exchange. The report is funded, partially or entirely, by a grant from the U.S. Department of Transportation's University Transportation Centers Program. However, the U.S. Government assumes no liability for the contents or use thereof.

Abstract

This report summarizes the second phase of an investigation on the performance of earthquake-damaged reinforced concrete bridges with repaired columns. In Phase II, a study was conducted to optimize the level of (pre-earthquake) retrofit of RC bridge columns that can be rapidly repaired (i.e., in a 3-day period) in the event of an earthquake. Retrofit and repair of earthquake-damaged reinforced concrete (RC) bridge columns have been studied extensively in the past several years; however, no studies have been conducted on the optimization process on the combined levels of retrofit and rapid repair. In this study, a framework is presented to optimize the combined levels of retrofit and rapid repair needed to maintain the level of serviceability of a bridge effected by an earthquake. Numerical simulation was used to model the response of two RC bridge columns with different reinforcement details and retrofitted with different methods that were reported in the literature. Incremental dynamic analysis (IDA) was used to determine the seismic response of a prototype bridge system that included the retrofitted RC columns to determine how different methods and levels of column retrofit affect the system-level response of the bridge structure and its ability to be repaired after an earthquake. Knowledge of the system-level performance can, in turn, be used to manage the levels of retrofit and repair to help ensure the survival of the infrastructure while reducing initial costs.

Chapter 1 Introduction

Reinforced concrete (RC) bridge columns are typically designed to be the primary source of energy dissipation for a bridge structure during an earthquake. According to current seismic design practice, RC bridge columns can experience different types of damage to the concrete (cracking, spalling, or crushing) or reinforcing bars (yielding) depending on the performance level of a bridge specified by the bridge owner or administrative agency. In an extreme scenario, bar buckling or fracture may also occur when the earthquake effects exceed the ultimate limit state. Therefore, seismic retrofit and repair of RC bridge columns have been investigated in many studies.

Structural retrofit and repair techniques include injection of concrete cracks (French et al. 1990), replacement of damaged concrete, and/or the application of external reinforcement, typically in the form of jackets. The most common jacketing materials are RC (Lehman et al. 2001), steel (Fukuyama et al. 2000), and fiber reinforced polymer (FRP) (Vosooghi and Saiidi 2009). The selection of the appropriate technique depends on the level of performance that can be achieved, cost, long term-durability (important for retrofit), and time/ease of installation (important for rapid repair).

Application of techniques of retrofit of RC bridge columns usually focus on increasing the strength, stiffness, and energy dissipation capability of the member. However, changes in column performance can influence the bridge structure performance in an unpredictable way, especially under seismic load. Therefore, minimizing the use of retrofit at the member level can decrease uncertainties related to the behavior of the bridge structure. On the other hand, reducing the level of retrofit considerably - or avoiding it altogether - can expose the structure to more damage to the point of causing the collapse. The objective of this study is to explore the

possibility of optimizing the level of column retrofit such that the bridge structure can withstand the earthquake without collapse, while suffering minor or moderate damage that can be rapidly repaired later.

Recent studies in the technical literature on repair have demonstrated that different techniques can be a viable option for restoring the use of earthquake-damaged RC bridge columns, even those columns that have been severely damaged. Further, studies have confirmed the feasibility of implementing certain repair techniques within a short timeframe (i.e., less than 3 days), thereby making them suitable for the purpose of rapid repair. A guide for the selection of rapid repair systems for earthquake-damaged columns is reported by Sneed et al. (2019). A proper management of levels of retrofit and repair techniques can therefore help ensure the survival of the infrastructure while reducing initial costs.

This report summarizes the Phase II work of a project aimed to study the system-level seismic response of an RC bridge with repaired or retrofitted columns. Phase I of the project studied the influence of a column repair (member level) on the post-repair performance of a bridge structures (system level) (Fraioli and Sneed 2021). In Phase II of the project, a methodology was developed to optimize the combined levels of (pre-earthquake) retrofit and (post-earthquake) rapid repair in order to maintain service to a bridge shortly after an earthquake occurs while reducing initial costs and uncertainties. The influence of the column member level retrofit on the performance of the bridge system was investigated using data from experimental studies conducted on RC bridge columns. Two large-scale RC bridge column tests with different retrofit methods were selected from the literature. Numerical models were developed using Open System for Earthquake Engineering Simulation (OpenSees) (McKenna et al. 2000) and were validated by comparing the calculated responses with the measured test data. The influence of

the member-level response on the bridge system response was investigated using numerical simulation of a prototype bridge structure developed in Phase I of this project (Fraioli and Sneed 2021). Finally, incremental dynamic analysis (IDA) was conducted to evaluate the seismic performance of an RC bridge structure that included one or more retrofitted columns with the aim of developing a framework to optimize the level of (pre-earthquake) retrofit of RC bridge columns that can be rapidly repaired (i.e., in a 3-day period) in the event of an earthquake.

Chapter 2 Modeling of RC Bridge Columns

2.1 Overview

This section presents the numerical models of the control (i.e., not retrofitted) and retrofitted columns considered in Phase II of this study. Two large-scale RC bridge column tests were selected from the literature to be modeled using the Open System for Earthquake Engineering Simulation (OpenSees) software framework (McKenna et al. 2000). Specimens selected for modeling were flexure-dominated and had the full hysteretic response of both the control and retrofitted columns reported so that the numerical model of the columns could be validated. In addition, all dimensions, material properties, and test characteristics were reported. The two columns had different internal reinforcement details resulting in different failure modes of the un-strengthened columns. Different techniques and materials were used to retrofit the two columns. The RC columns were modeled with the intent to evaluate the performance of the different retrofit strategies. The developed column models were then implemented in a model of a prototype bridge structure to investigate the seismic response of the bridge structure with retrofitted columns.

2.2 Modeling of the Control and Retrofitted Columns

Both the control and retrofitted columns were modeled as non-linear beam-column elements with a fiber section object, in which the cross section is discretized into fibers, since studies have shown that the fiber element method can be effective in simulating the response of RC members under seismic loading (Shao et al. 2005, Zhu et al. 2006, Xiao and Ma 2005). Each fiber is characterized by a prescribed uniaxial material, an area, and a location. The core concrete, cover concrete, and longitudinal steel fibers were defined by a uniaxial stress-strain model corresponding to the material they represent.

Confined and unconfined concrete were modeled in OpenSees using Linear Tension Softening Concrete02 material. The compressive stress–strain relationship of the material model is based on the uniaxial Kent–Scoff–Park concrete material model (Kent and Park 1971). The tensile stress–strain relationship is bilinear with the same modulus as the compressive elastic modulus. The effect of the confinement caused by the internal transverse reinforcement and by steel or FRP jacket was evaluated using Mander's model (Mander et al. 1988). Figure 2.1 shows the stress-strain relationship and required input values.
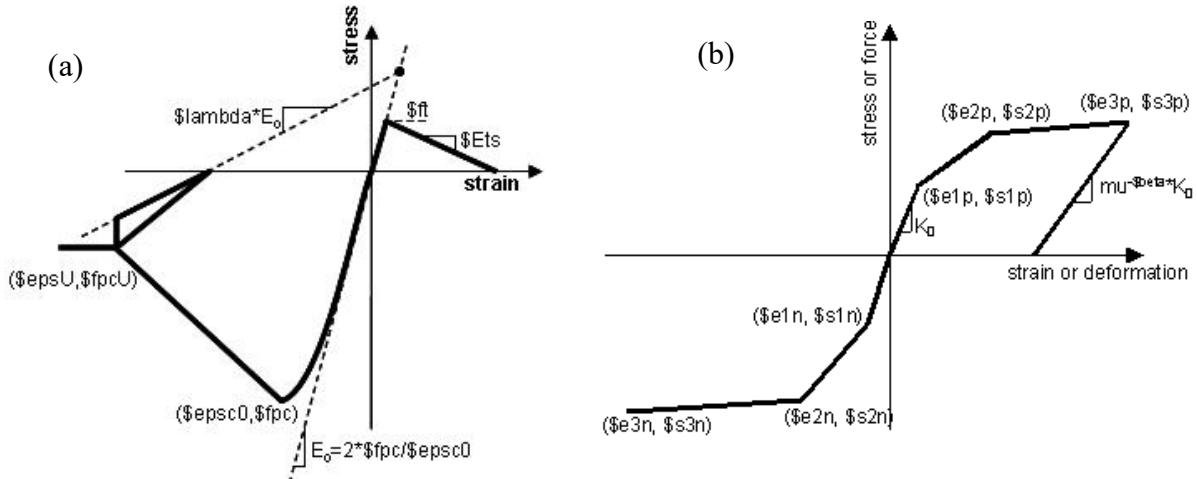
Figure 2.1 (a) Concrete02 Material – Linear Tension Softening, (b) Hysteretic Material (right) (Mazzoni et al. 2006)

The longitudinal reinforcing steel was modeled in OpenSees as Hysteretic material. This model was selected based on the capability to simulate the strength degradation due to bar fracture or buckling and to achieve convergence at large strains (He et al. 2016). The hysteretic material model requires three stress–strain inputs in both tension and compression to represent the monotonic behavior of the reinforcing steel. The cyclic behavior of the steel model is

controlled by additional parameters px (pinching factor for strain during reloading), py (pinching factor for stress during reloading), D1 (damage due to ductility), D2 (damage due to energy), and β (power used to determine the degraded unloading stiffness based on ductility). The behavior of reinforcing steel in tension and compression was modeled with the same values. Figure 2.1 shows the stress-strain relationship and required input values.

The total lateral deflection of an RC column under lateral load is attributed to flexural, shear, and bond slip deformations (Scott et. al 1982, Paulay and Priestley 1992). Shear and bond slip deformations were simulated by using zero-length springs, referred to as shear and bond–slip springs, respectively. The shear spring was modeled as a ZeroLength element in OpenSees. The force–deformation relationship in the loading direction was modeled with the Hysteretic material. The force–deformation relationships in the other directions were modeled with elastic materials with a large elastic stiffness that approaches infinity to exclude the flexibility in those directions. The pinching effect and strength degradation were neglected in the cyclic behavior of the shear spring, and the unloading stiffness was kept as the initial elastic stiffness. The unloading stiffness in the shear spring cyclic behavior was kept as the initial elastic stiffness. A bond–slip spring, modeled as a ZeroLengthSection element, was used to take into account the bond slip from strain penetration effects. The bond-slip spring had the same section discretization of the column element, but a stress-slip relationship was used to characterize the reinforcing steel. According to Zhao and Sritharan (2007), the relationship of bar stress versus loaded-end slip can be assumed as a linear relationship for the elastic region and a curvilinear relationship for the post-yield region.

2.3 Column A

2.3.1 Experimental description and column response

The first test selected for the simulation was carried out by Xiao and Ma (1997). The control test specimen, named C1-A in the reference, was 2642 mm high and had a circular cross-section of 610 mm. Figure 2.2 shows the dimensions of the column and the layout of the internal reinforcement.
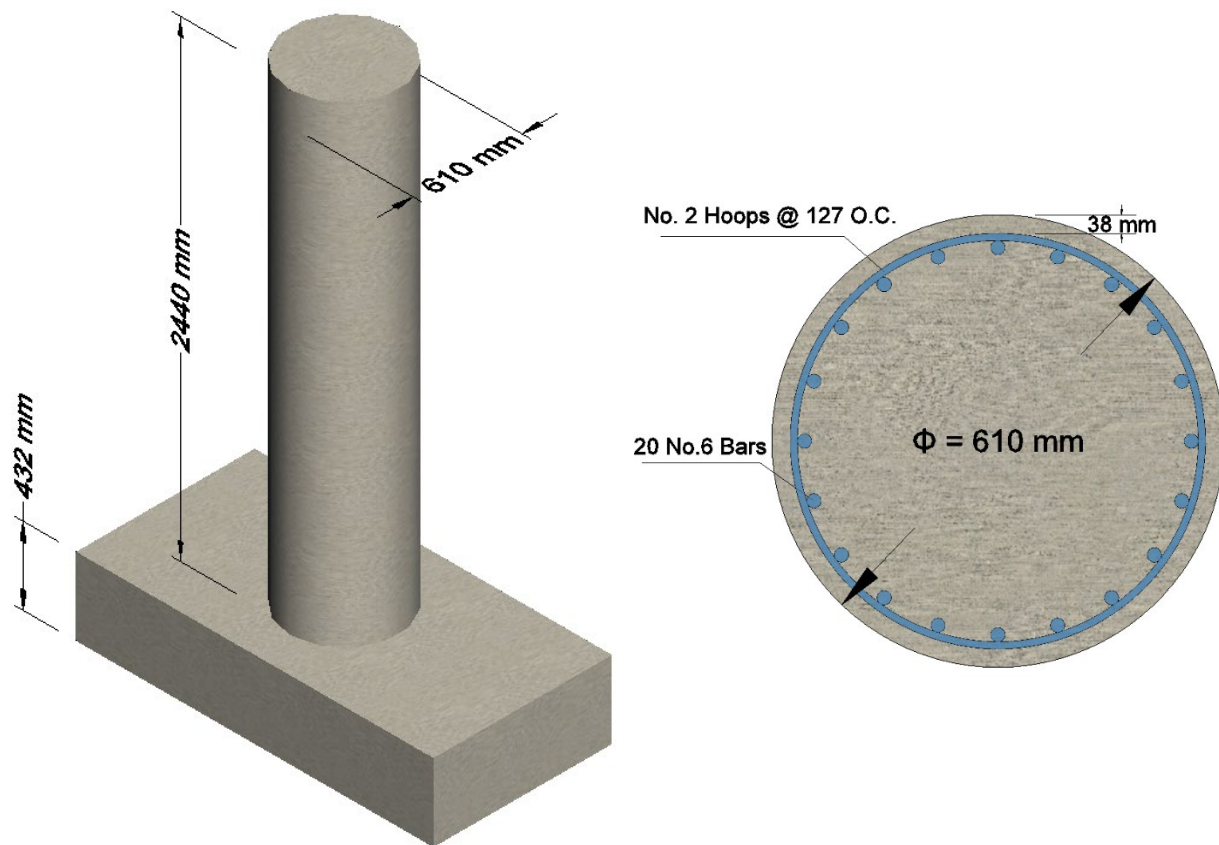

Figure 2.2 Column A: column and cross-section dimensions of specimens tested by Xiao and Ma (1997)

The column was reinforced using 20 No. 6 (nominal diameter 19.1 mm) Grade 60 bars (yield strength 462 MPa), for a longitudinal reinforcement ratio of 2% of the gross area of the

column section. The longitudinal steel bars were lap-spliced at the bottom of the column with the starter bars in the footing with a lap length of 381 mm. The transverse reinforcement consisted of No. 2 (nominal diameter 6.4 mm) hoops spaced at 127 mm. Concrete 28-day cylindrical strength was 44.8 MPa.

The test setup was designed to subject the column to cyclic lateral forces in a single curvature condition while applying a constant compressive axial load of 712 kN, corresponding to a ratio $(P/f'_c A_g)$ of 5%. The axial load ratio was considered in the appropriate range to simulate the column condition of a typical multicolumn bent bridge (Xiao and Ma 1997). The lateral load sequence, shown in Figure 2.3, was controlled by displacement increments based on the reference ductility index. The initial loading cycles were applied corresponding to a peak displacement in increments of 2.5 mm, until the column developed the calculated capacity corresponding to the first yielding of the longitudinal bars. After the column developed the yield capacity, three complete loading cycles were performed corresponding to 1μ, 1.5μ, 2μ, 3μ, 4μ, 6μ, and 8μ, where μ indicates the displacement ductility factor defined as the ratio of displacement, Δ, to the reference yield displacement, Δ_y.

Failure of the control column occurred due to insufficient lap-splice between the longitudinal reinforcement and starter bars. Flexural cracks appeared at the bottom of the column when the test reached a lateral displacement of 5 mm, which then extended to the whole lap splice region at a displacement of 13 mm. At a displacement of 28 mm, the first vertical crack appeared in the lap-splice region, indicating the initiation of the bond slip. After reaching a displacement of 41 mm, vertical cracks were fully spread in the lap splice region, indicating complete bond-slip failure. The test was terminated at a displacement of 61 mm when the lateral force capacity dropped to 50% of the maximum capacity equal to 231 kN.
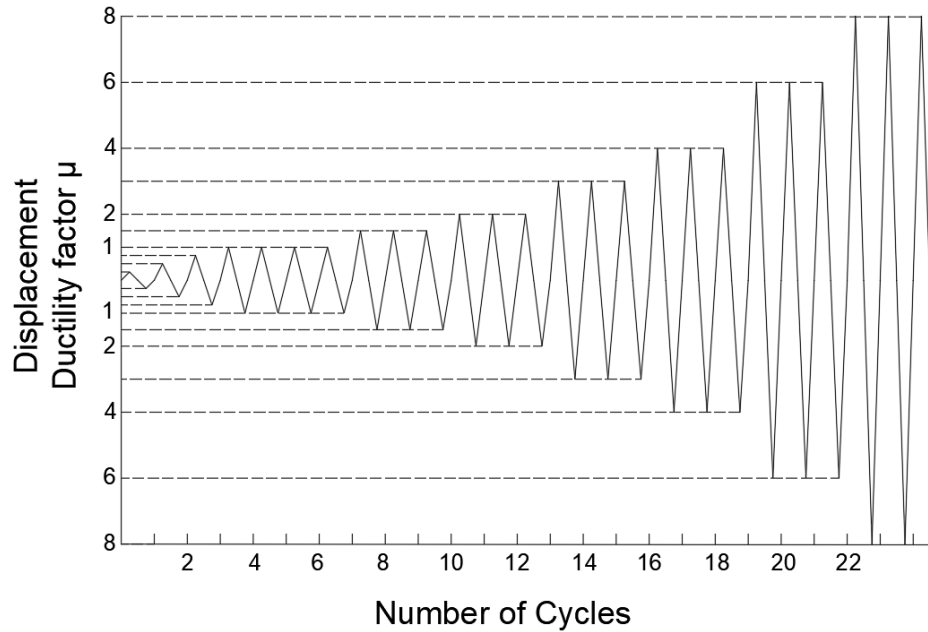
Figure 2.3 Column A: specified displacement history

The retrofitted test specimen, named C3-RT5 in the reference (Xiao and Ma 1997), was reinforced using a prefabricated GFRP jacket. The jacket consisted of multiple layers of unidirectional glass fibers arranged with 90% fibers oriented in the hoop direction and 10% fibers oriented in the longitudinal direction, embedded in a 2-part epoxy. The reported elastic modulus and ultimate strength in the circumferential direction were 48300 MPa and 552 MPa, respectively. Five layers of composite were used to reinforce the lower portion of the column up to 1220 mm to maximize flexural enhancement, while three layers were used to wrap the above portion for an additional height of 991 mm. Urethan-based high strength adhesive was used to bond the prefabricated composite shells forming a continuous jacket. A 19 mm gap was intentionally provided between the footing and the bottom of the jacket.

The retrofitted column was tested using the same cyclic test protocol used for the control column. During the test, flexural cracks were observed at the column base, where the gap was

left. At higher deformation, corresponding to a displacement ductility factor of 8 and to an approximate drift ratio of 5%, fine horizontal cracks were observed on the surface of the composite jacket that were attributed to the smaller fiber content in the longitudinal direction. Deterioration of the bond in the lap splice region was observed as consequence of the pullout of the starter bars. Nevertheless, no delamination or rupture of the jacket was observed during the test. The retrofit method proved to be capable of increasing both the load-carrying capacity and ductility. Figure 2.4 shows the cyclic behavior of both the control and retrofitted columns.
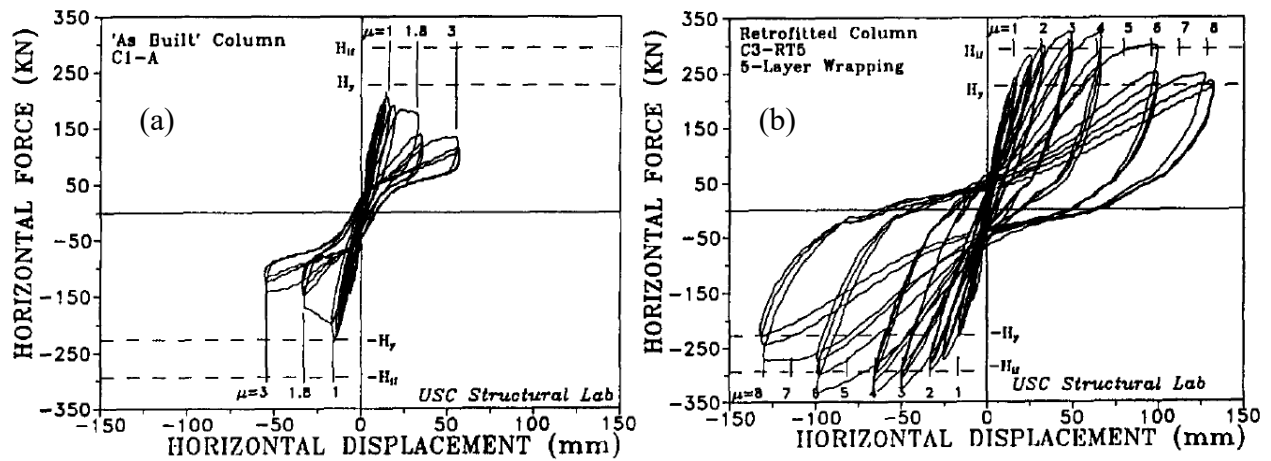
Figure 2.4 Column A: (a) cyclic behavior of control column, (b) cyclic behavior of retrofitted column (Xiao and Ma 1997)

2.3.2 Column numerical model and validation

Both the control and retrofitted columns were modeled as a non-linear beam-column element with a fiber cross-section consisting of 7 subdivisions (fibers) in the circumferential direction and 12 subdivisions (fibers) in the radial direction. Figure 2.5 shows the column model and cross-section discretization. The retrofitted column, represented in Figure 2.6, was wrapped by 5 or 3 layers of GFRP jacket along the length. Therefore, the cross-section was subdivided

10

into two macro areas: the cover confined by the GFRP jacket, and the core confined by both the transverse reinforcement and the GFRP jacket.
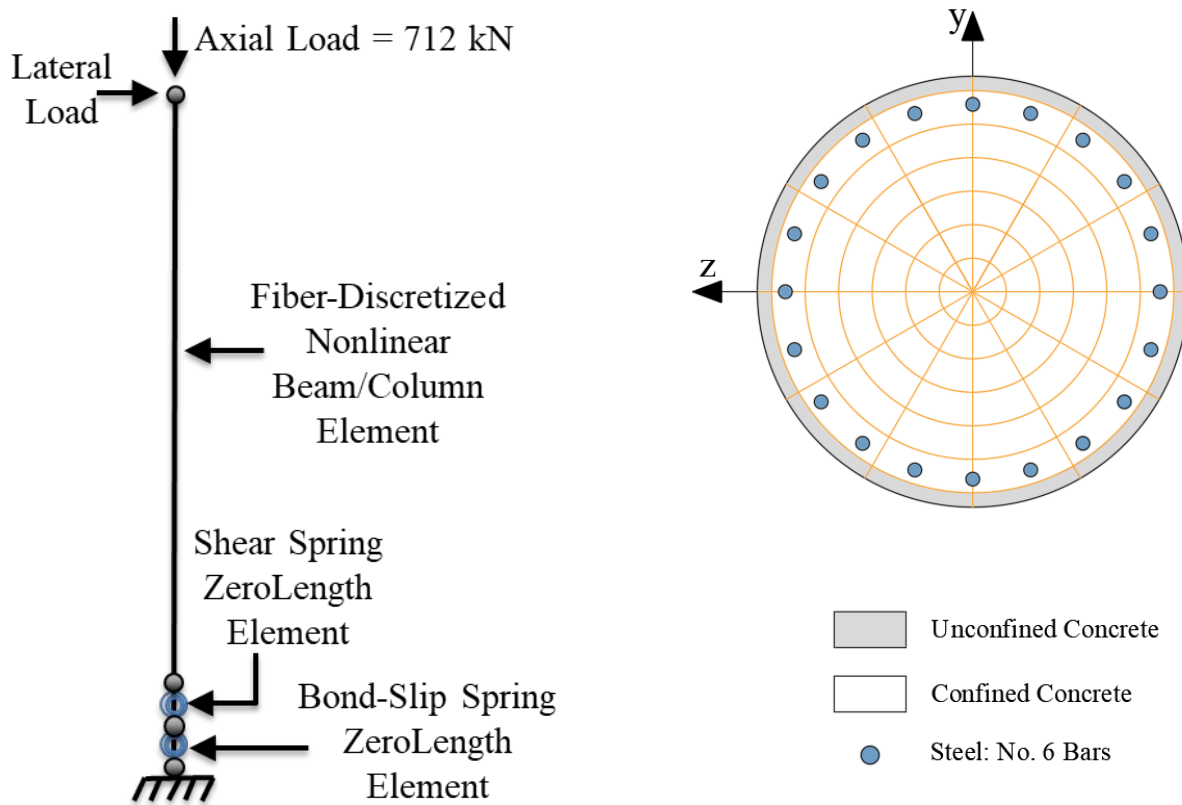
Figure 2.5 Column A: control column and cross section model

The experimental cyclic test carried out on Column A was modeled in OpenSees according to the description in Section 2.2. The software was run on a workstation with an Intel Xenon processor with a speed of 3.6 GHz on a 64-b operating system. The program took approximately 1 minute. The results were obtained by plotting OpenSees output text files using MATLAB. In Figures 2.7 and 2.8 the numerical results of Column A are shown and compared with the experimental cyclic response. The numerical results are in good agreement with the

11

experimental results. These results show the retrofitted column can be simulated using the proposed approach.
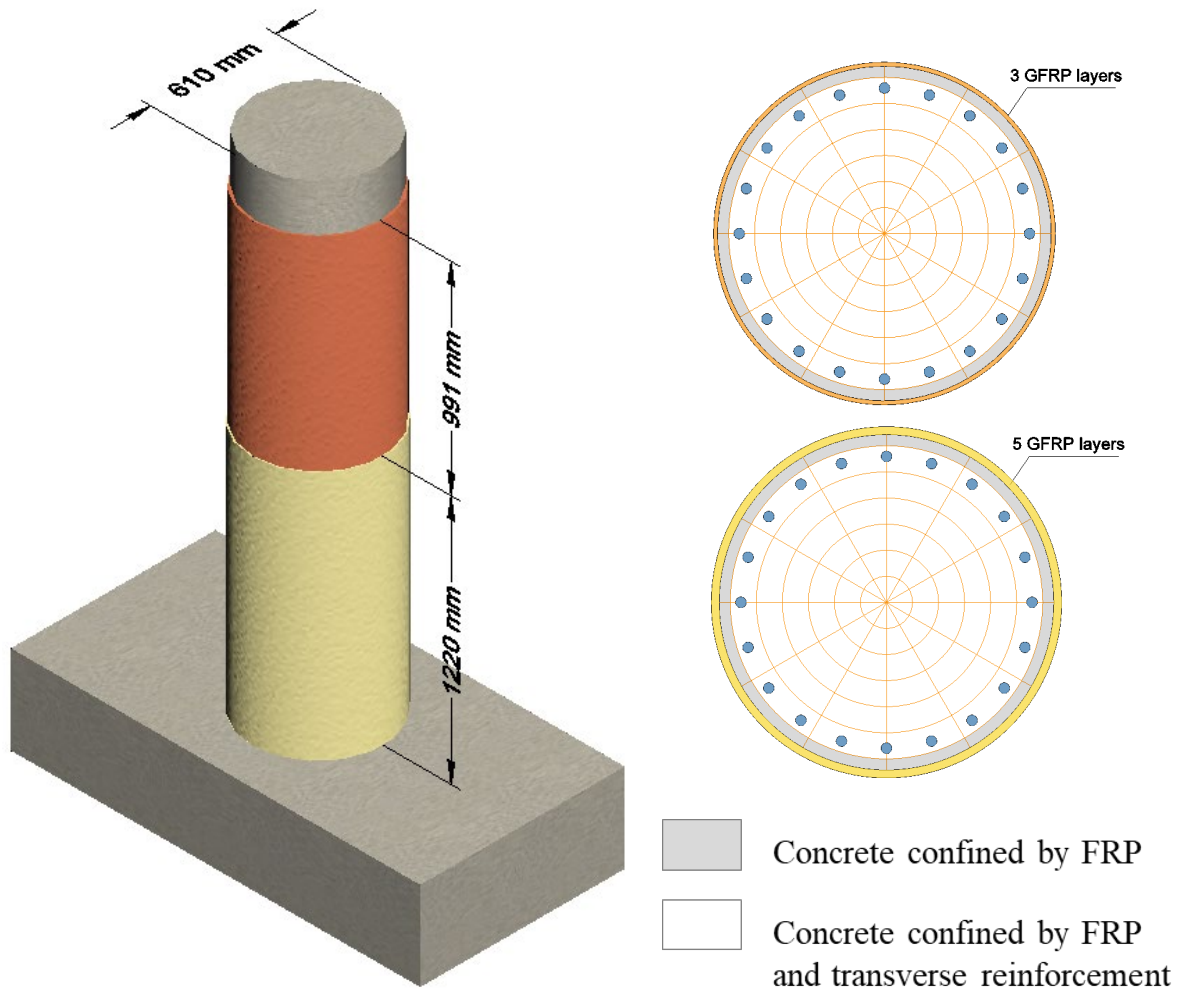
Figure 2.6 Column A: retrofitted column and cross section model
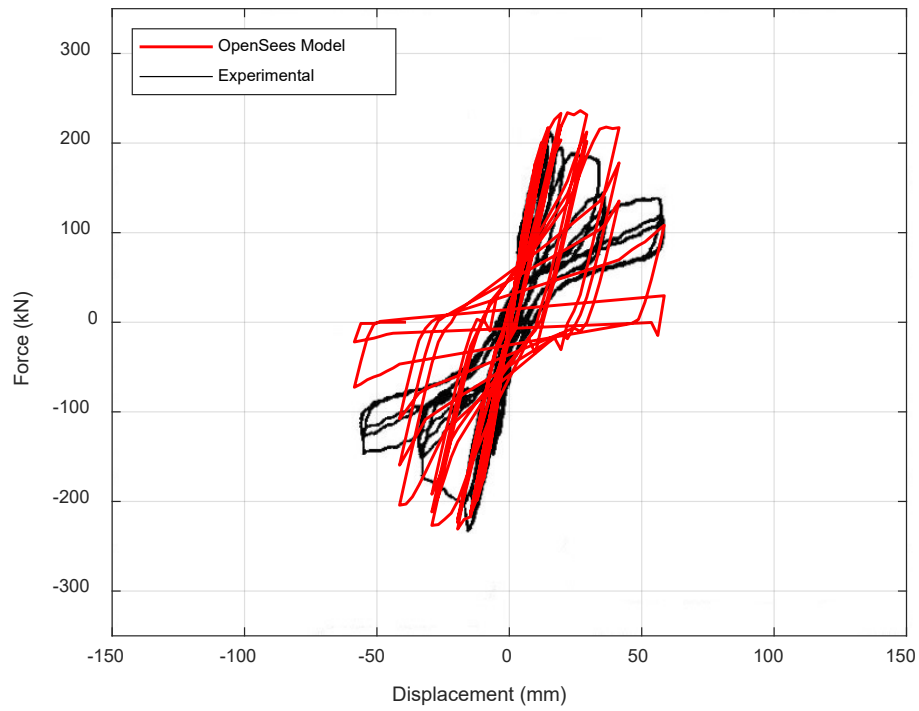
Figure 2.7 Column A: numerical and experimental cyclic behavior of control column
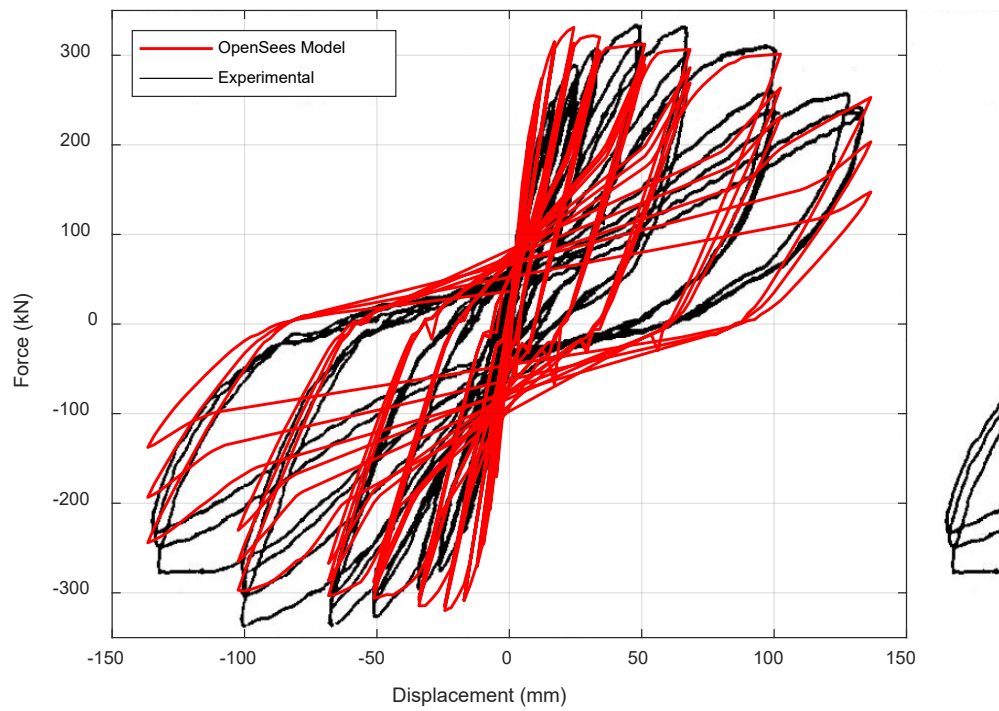
Figure 2.8 Column A: numerical and experimental cyclic behavior of retrofitted column

13

2.4 Column B

2.4.1 Experimental description and column response

The second test selected for the simulation was carried out by Chai et al. (1991). The control column, identified as Test Unit 3, was 3657 mm high and 610 mm in diameter. The cross-section longitudinal reinforcement consisted of 26 No. 6 (12.7 mm dia.) Grade 40 reinforcing steel bars (yield strength 315 MPa), while the transverse reinforcement consisted of No. 2 (6.4 mm dia.) Grade 40 circular hoops placed at 127 mm. The longitudinal reinforcement ratio was 2.53%, while the corresponding confining steel ratio was 0.18%. The continuous longitudinal bars were anchored with 90-degree hooks in the footing. Concrete was designed with a target compressive strength of 34.5 MPa. Figure 2.9 shows the column dimensions and the location of reinforcement in the cross-section.
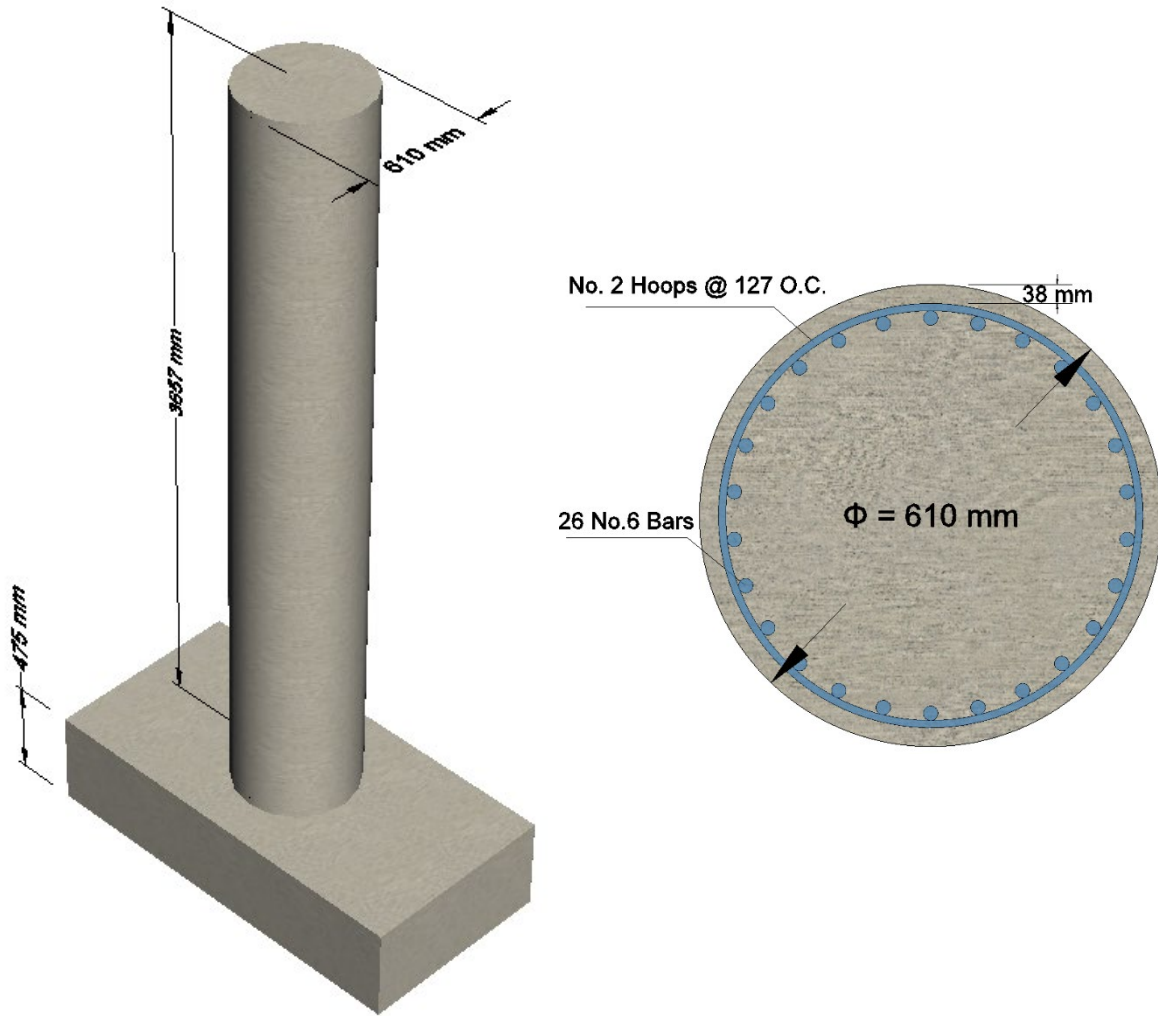
Figure 2.9 Column B: column and cross-section dimensions of the specimens tested by Chai et al. (1991)

A vertical load of 1780 kN was applied to the test column, which corresponds to an axial load ratio of (P/f'$_c$'A$_g$) of 18%, while the column was subjected to the lateral displacement pattern of increasing magnitude shown in Figure 2.10. The yield displacement Δ_y corresponds to the theoretical first yield of the extreme tension steel bar.
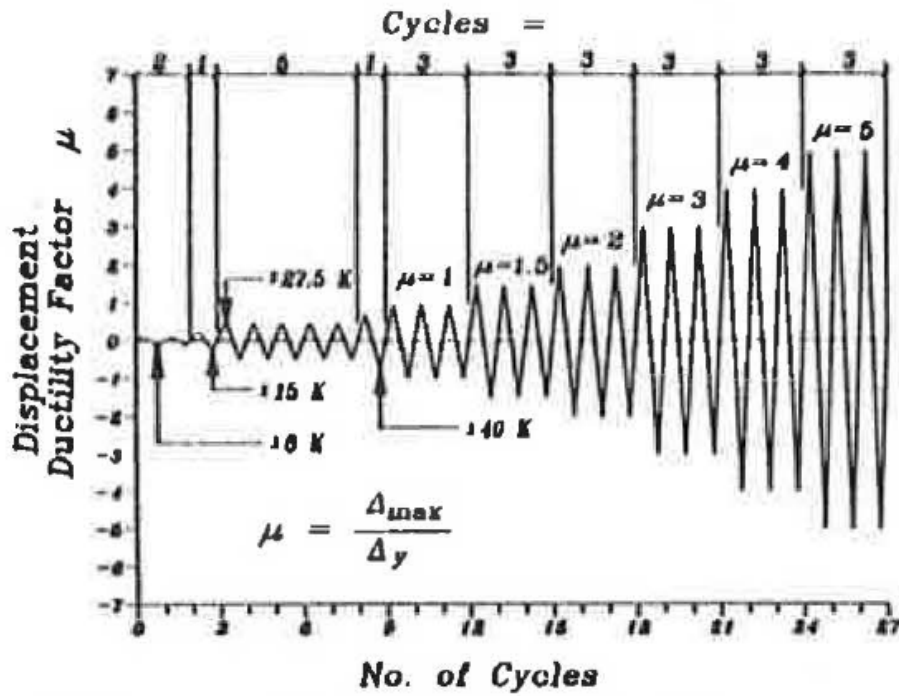
Figure 2.10 Column B: specified displacement history (Chai et al. 1991)

Failure of the control column occurred due to buckling of the longitudinal reinforcement corresponding to a maximum displacement ductility factor of $\mu = 5$. Before failure, very little degradation in flexural strength was noted between cycles of the same displacement magnitude. The retrofitted test, named Test Unit 4, was reinforced using a steel jacket fabricated from a 4.76 mm thick A36 hot-rolled steel. A 6.35 mm gap was provided between the column and the jacket and was pressure-injected with a cement grout. The cement grout compressive strength was evaluated using 51 mm diameter cylinders and ranged between 14 MPa and 17 MPa at an age of 14 days. To avoid bearing the jacket against the footing, a gap of 25 mm was provided between the jacket and the footing. The jacket was 1219 mm high to ensure the moment demand immediately above the jacket would not exceed 75% of the unjacketed flexural capacity.

16

The retrofitted column was tested using the same cyclic test protocol used for the control column. In comparison with the control column, the Test Unit 4 showed significant increase in both flexural strength and ductility, reaching a maximum displacement ductility factor $\mu = 8$ in the push direction, corresponding to a drift ratio of 6%. The displacement ductility in the pull direction reached a maximum of $\mu = 6.7$ due to test setup limitation. Failure was caused by low-cycle fatigue fracture of the extreme tension reinforcement. Figure 2.11 shows the cyclic behavior of both the control and retrofitted columns.
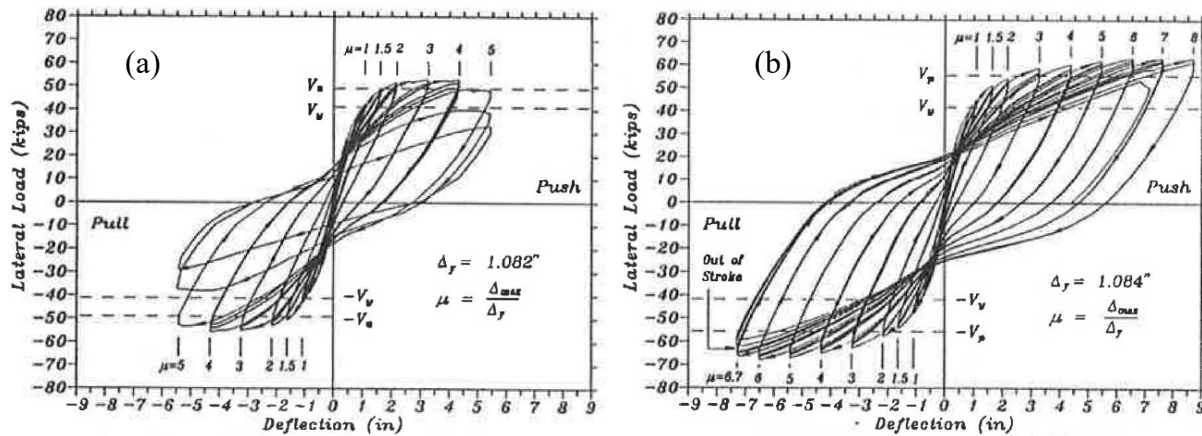
Figure 2.11 Column B: (a) cyclic behavior of the control column, (b) cyclic behavior of retrofitted column (Chai et al. 1991)

2.3.2 Column numerical model and validation

Both the control and retrofitted columns were modeled as a non-linear beam-column element with a fiber cross-section consisting of 7 subdivisions (fibers) in the circumferential direction and 12 subdivisions (fibers) in the radial direction. Figure 2.12 shows the column model and cross-section discretization. The retrofitted column, shown in Figure 2.13, was confined by a steel jacket. Therefore, the cross-section was subdivided into two macro areas: the

cover confined by the steel jacket, and the core confined by both the transverse reinforcement and the steel jacket.
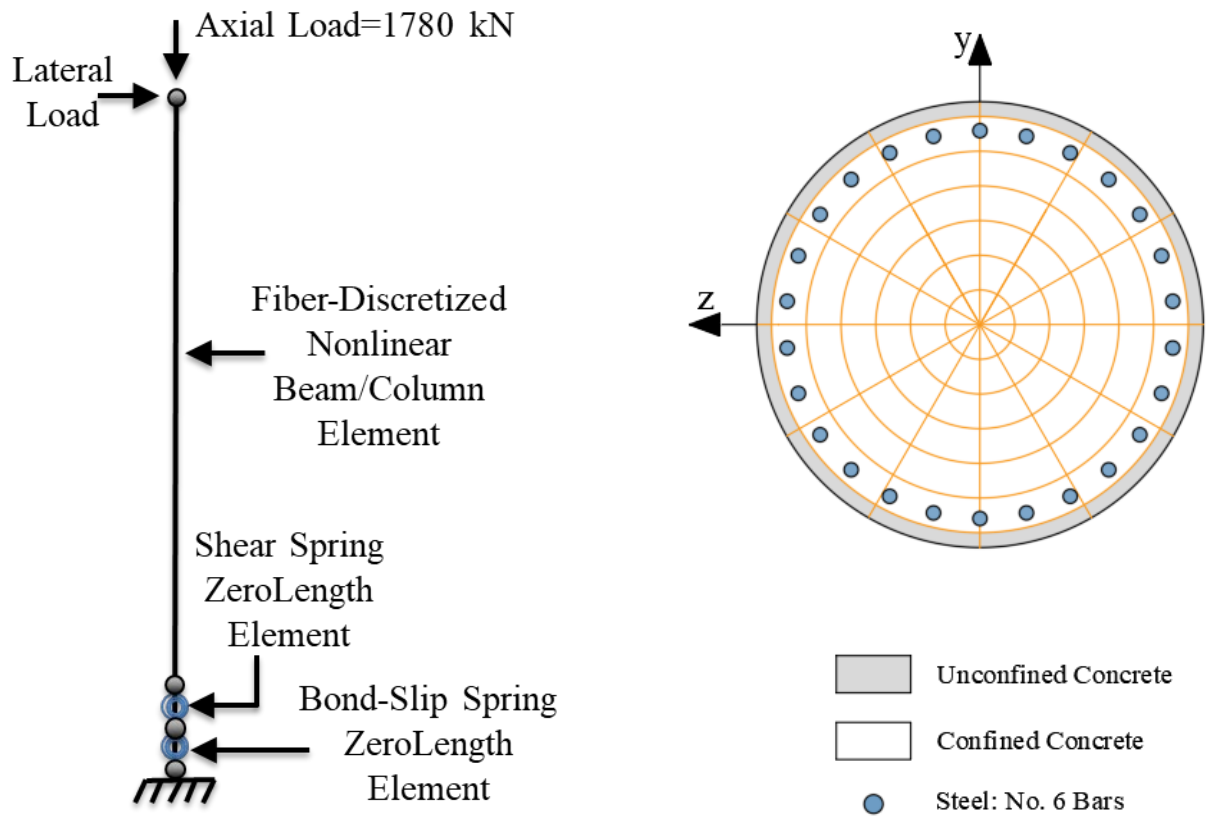
Figure 2.12 Column B: control column and cross section model
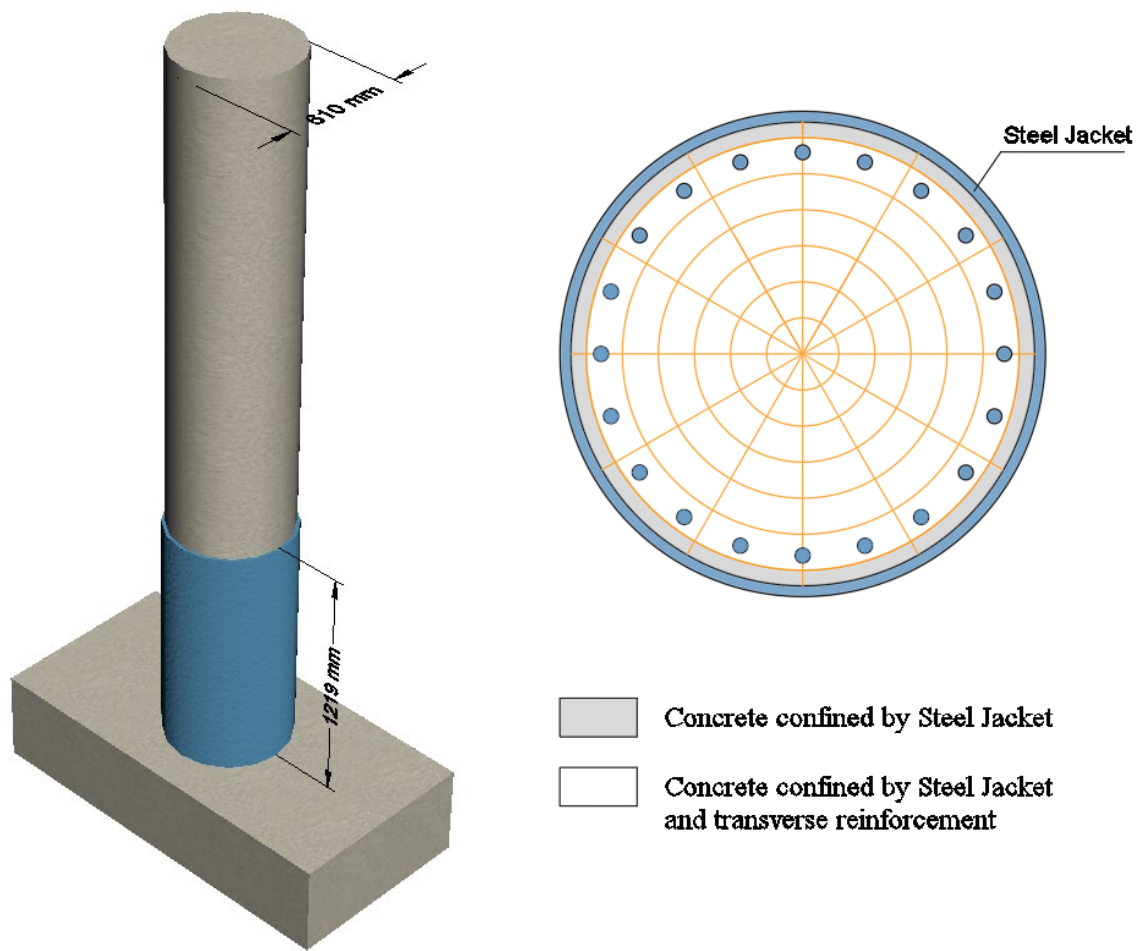
Figure 2.13 Column B: retrofitted column and cross section model

The experimental cyclic test carried out on Column B was modeled in OpenSees according to the description in Section 2.2. The software was run on a workstation with an Intel Xenon processor with a speed of 3.6 GHz on a 64-b operating system. The program took approximately 1 minute. The results were obtained by plotting OpenSees output text files using MATLAB. In Figures 2.14 and 2.15 the numerical results of Column B are shown and compared with the experimental cyclic response. The numerical results are in good agreement with the experimental results. These results show the retrofitted column can be simulated using the proposed approach.
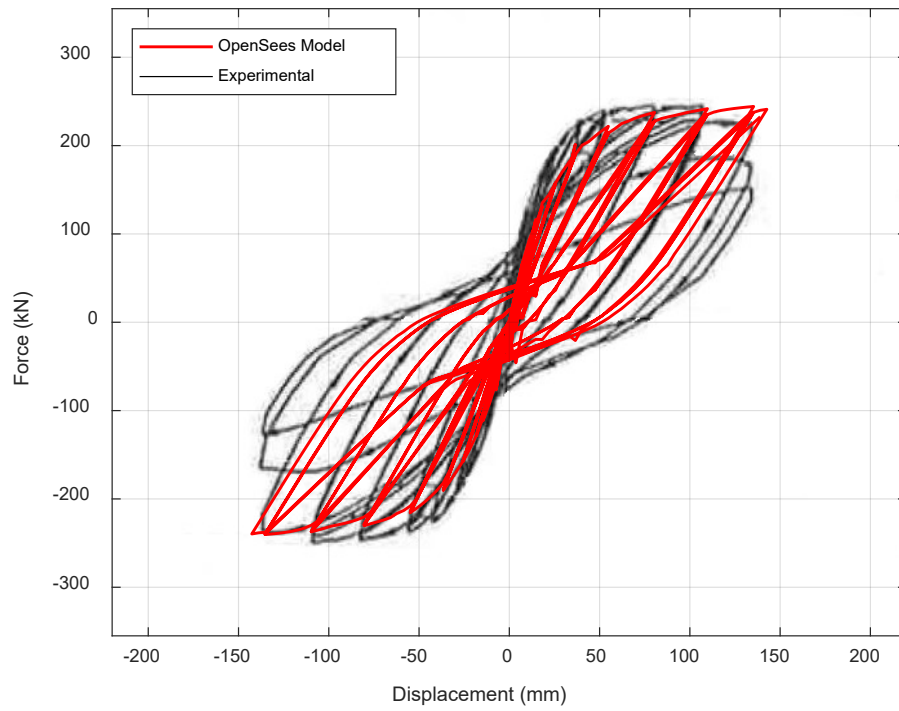
Figure 2.14 Column B: numerical and experimental cyclic behavior of control column
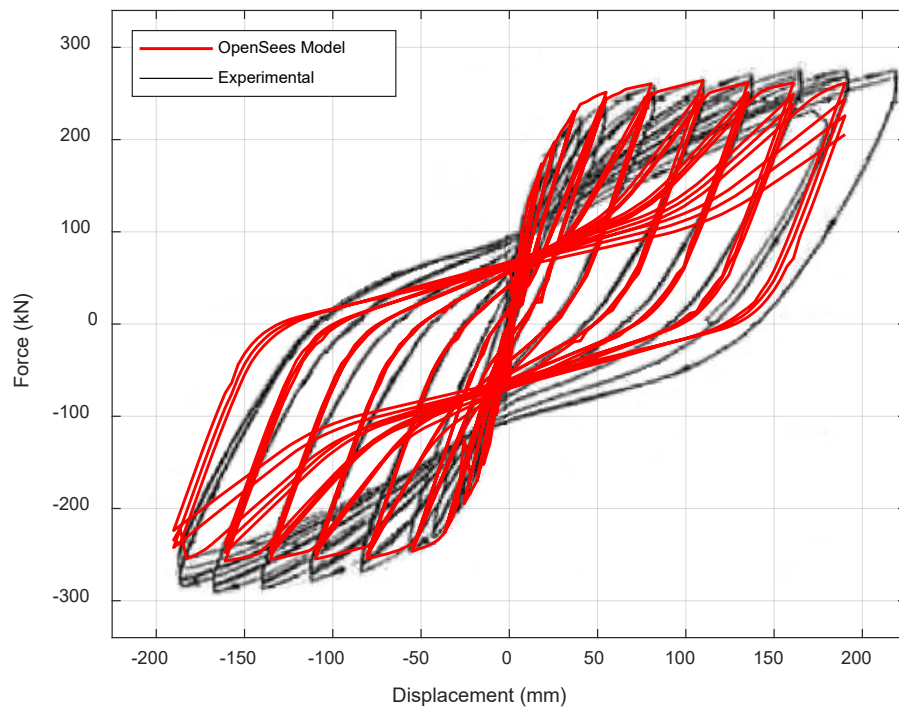
Figure 2.15 Column B: numerical and experimental cyclic behavior of retrofitted column

20

Chapter 3 Behavior of RC Bridge Structure

3.1 Overview

This section presents the numerical results of the RC bridge structure models with control

columns considered in this study. A prototype bridge was selected to be modeled using the

OpenSees software framework (McKenna et al. 2000). The control column models developed in

Chapter 2 were implemented into the bridge structure model with the intent to evaluate the

seismic response of the bridge structure and then examine how retrofitted RC columns effect the

system-level response. Ground motion records were selected from the Pacific Earthquake

Engineering Research Center (PEER) Strong Motion Database and applied to the bridge

structure model using incremental dynamic analysis (IDA). The aim of the dynamic analysis was

to generate IDA curves of the intensity measure (IM) vs. damage measure (DM) for the selected

ground motion records. A 5% damped first mode spectral acceleration Sa(T1,5%) (where T1 is

the period of the 1st mode response) was adopted as the IM, and the maximum drift ratio was

adopted as the DM.

3.2 RC Bridge Structure Model and Validation

A three-span RC bridge structure provided by the Federal Highway Administration

named *Seismic Design of Bridges – Design Example No. 4* (FHWA 1996) was modeled in

OpenSees. The prototype bridge described herein is the same as that simulated in Phase I of this

study (Fraioli and Sneed 2021). The bridge had RC columns with a geometry (in terms of cross-

sectional shape and aspect ratio) similar to those simulated in Chapter 2. The superstructure was

designed with continuous span of lengths 3048 cm, 3657 cm, and 3048 cm. The 30-degree skew

between the superstructure and bents was not considered since the skew effect was not the focus

of this study. Figure 3.1 shows an illustration of the prototype bridge model.
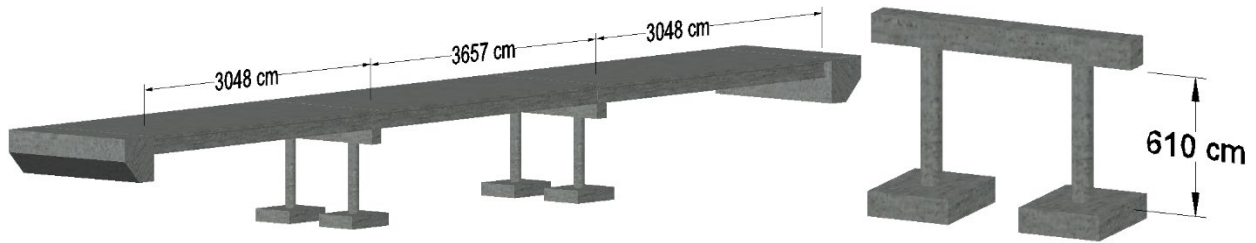
Figure 3.1 Design example No. 4 bridge dimensions

The RC bridge columns had a height of 610 cm and a circular cross-section with 122 cm

diameter. The columns were reinforced with 34 ASTM 706 Grade 60 No. 11 (35 mm dia.)

longitudinal bars, and No. 5 (16 mm dia.) spirals at a spacing of 89 mm with a concrete cover of

50 mm. The resulting longitudinal and transverse reinforcing ratios were 2.79% and 0.8%,

respectively. The effective height of the columns was 713 cm from the top of the footing to the

centroid of the gross cross-section of the box girder, with a resulting aspect ratio of 5.85 for the

columns. According to the design example (FHWA 1996), the bridge was designed for seismic

loading using the Standard Specification for Highway Bridges (AASHTO 1995). The bent

columns were designed to be cast in place (CIP) monolithically with the CIP box girder resulting

in a nearly fixed joint between the superstructure and the substructure.

The bridge was modeled using OpenSees with a 1/2–scale to be adapted to fit the

dimensions of the RC columns chosen previously (Chapter 2). The superstructure model

consisted of 12 elements, four elements per span, located in a single line along the centerline of

the bridge structure. The moment of inertia and the torsional stiffness of the superstructure were

determined based on gross cross-sectional properties. The mass density of the superstructure was

adjusted so the fundamental frequency remained the same as the full-scaled bridge. Figure 3.2

shows the numerical model of the scaled bridge structure in OpenSees.
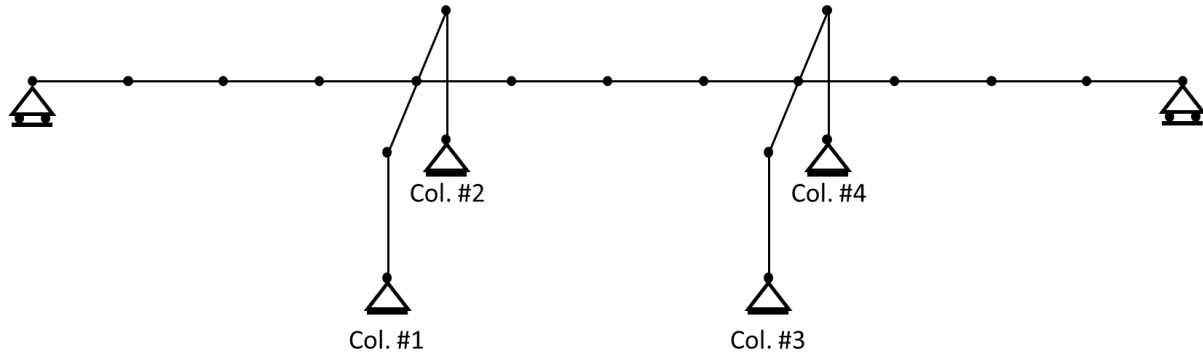
Figure 3.2 Numerical model of the scaled bridge structure

For simplification purposes, the analysis focused on the response of the bridge structure

in a single direction corresponding to the predominant direction of the response. Modal analysis

was conducted to validate the numerical bridge model. The fundamental frequency of the model

including only original columns determined from the modal analysis was 1.236 Hz, which is

similar to the value provided for the full-scaled bridge in the example No. 4 (1.202 Hz), see

Figure 3.3.

```
PROGRAM SAP90, VERSION BETA6.00                FILE:exam4.OUT
FHWA BRIDGE NO 4 PRELIMINARY DESIGN CALCS

E I G E N V A L U E S    A N D    F R E Q U E N C I E S

    MODE      PERIOD     FREQUENCY    FREQUENCY    EIGENVALUE
              (TIME)     (CYC/TIME)   (RAD/TIME)   (RAD/TIME)**2

      1      0.831827    1.202172     7.553472     57.054941
      2      0.492683    2.029703    12.753000    162.639019
      3      0.297626    3.359927    21.111042    445.676084
      4      0.229760    4.352366    27.346720    747.843098
      5      0.208742    4.790611    30.100294    906.027677
      6      0.204992    4.878243    30.650903    939.477861
      7      0.125186    7.988121    50.190842    2519.121
      8      0.101884    9.815115    61.670188    3803.212
      9      0.082165   12.170569    76.469940    5847.652
     10      0.081362   12.290709    77.224804    5963.670
     11      0.076875   13.008090    81.732243    6680.160
     12      0.068666   14.563152    91.502984    8372.796
```

Figure 3.3 Example No. 4 modal periods and vibrations (FHWA 1996)
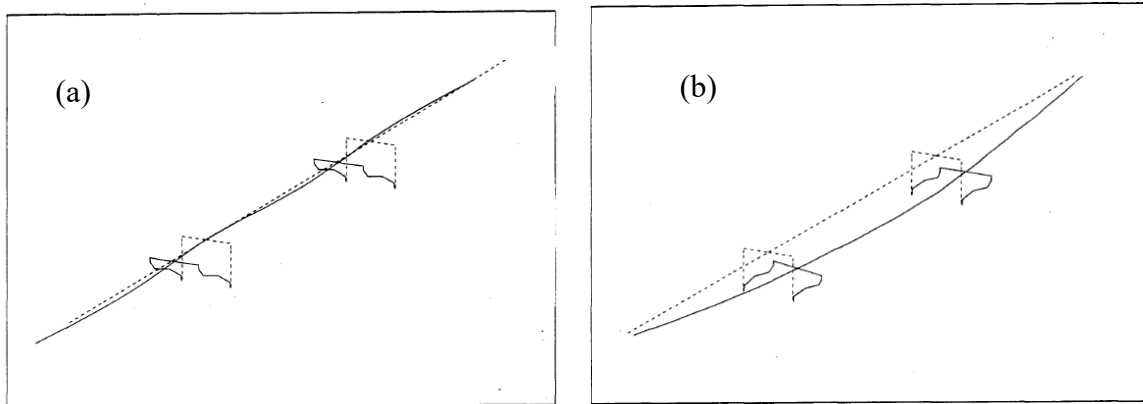
Figure 3.4 Example No. 4 deformed shapes for (a) mode 1, (b) mode 2 (FHWA 1996)

3.3 Modeling of RC Bridge Structure with Retrofitted Columns

3.3.1 Models considered

As the first step, the control bridge column models developed in Chapter 2 were

implemented into the bridge structure model. In this scenario, the control columns were modeled

as columns 1 to 4 defined in Figure 3.2 of the bridge model validated in Section 3.2. The model

with Column A control columns (Section 2.3) is referred to as Bridge A. The model with

Column B control columns (Section 2.4) is referred to as Bridge B. The bridge models were used

as the control to evaluate the effect of the column retrofit.

3.3.2 Selection of ground motion records

Twenty data sets of GM records from seven earthquakes were selected according to the

target design spectrum determined with (AASHTO 1995). The GM records selected herein were

the same as those selected in Phase I of this study (Fraioli and Sneed 2021). Each data set

included subsets of data in two orthogonal directions recorded from the same event and record

station resulting in 40 total GM records. The GM records were obtained from the database

provided by the Pacific Earthquake Engineering Research Center (PEER). The records were

selected among those with relatively large magnitudes of 6.5–7.0 and with moderate epicentral

distances of 15–31 km.

According to Bradley et al. (2006), the selected GM records were scaled to a spectral

acceleration of 1.0 g at the fundamental time period of the structure. Table 3.1 shows the

earthquake set with the relative PGA values. Figure 3.5 shows the spectral acceleration for the

selected GM records before and after scaling.

Table 3.1 Selected earthquake ground motion records

| Earthquake set	Event	Year	Station	Ma	Rrup (km)	Record no.	PGA (g)
1	San Fernando	1971	LA – Hollywood Stor FF	6.61	22.8	1	0.2248
						2	0.1949
2	Imperial Valley-06	1979	Cerro Prieto	6.53	15.2	3	0.1683
						4	0.1571
3	Imperial Valley-06	1979	Delta	6.53	22.0	5	0.2357
						6	0.3497
4	Imperial Valley-06	1979	El Centro Array #12	6.53	19.9	7	0.1449
						8	0.1181
5	Imperial Valley-06	1979	El Centro Array #13	6.53	22.0	9	0.1180
						10	0.1385
6	Irpinia -Italy -01	1980	Bisaccia	6.90	21.3	11	0.0955
						12	0.0825
7	Superstition Hills-02	1987	El Centro Imp. Co. Cent	6.54	18.2	13	0.3573
						14	0.2595
8	Superstition Hills-02	1987	Kornbloom Road (temp)	6.54	18.5	15	0.1139
						16	0.1390
9	Superstition Hills-02	1987	Wildlife Liquef. Array	6.54	23.9	17	0.1792
						18	0.2076
10	Spitak-Armenia	1988	Gukasian	6.77	24.0	19	0.2003
						20	0.1740
11	Loma Prieta	1989	Agnews State Hospital	6.93	24.6	21	0.1652
						22	0.1379
12	Loma Prieta	1989	Coyote Lake Dam (Downst)	6.93	20.8	23	0.1604
						24	0.1794
13	Loma Prieta	1989	Coyote Lake Dam (SW Abut)	6.93	20.3	25	0.1519
						26	0.4847
14	Loma Prieta	1989	Hollister – South & Pine	6.93	27.9	27	0.3699
						28	0.1787
15	Loma Prieta	1989	Hollister Diff. Array	6.93	24.8	29	0.2689
						30	0.2786
16	Loma Prieta	1989	Palo Alto – 1900 Embarc.	6.93	30.8	31	0.2146
						32	0.2047
17	Loma Prieta	1989	Palo Alto – SLAC Lab	6.93	30.9	33	0.1948
						34	0.2771
18	Loma Prieta	1989	Sunnyvale – Colton Ave.	6.93	24.2	35	0.2074
						36	0.2072
19	Northridge-01	1994	LA – Wadsworth VA Hospital North	6.69	23.6	37	0.1854
						38	0.1642
20	Northridge-01	1994	Playa Del Rey – Saran	6.69	24.4	39	0.1435
						40	0.0701
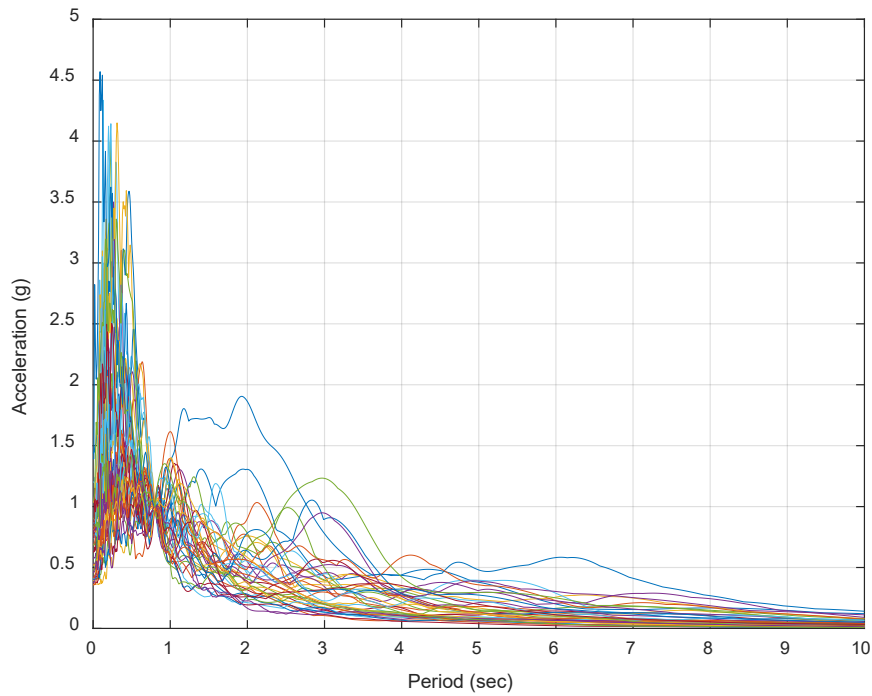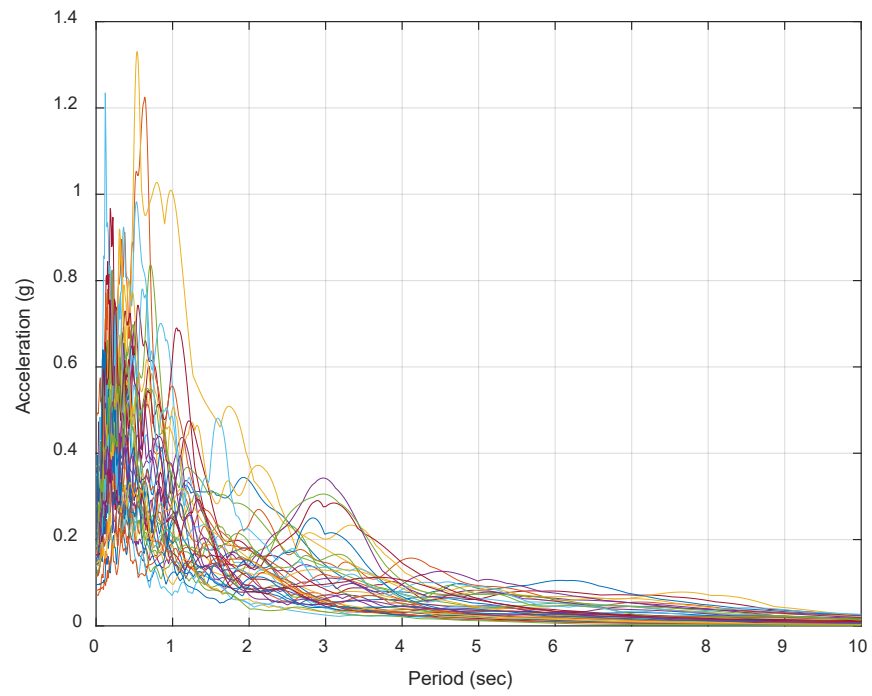
Figure 3.5 Spectral acceleration for the selected GM records: (a) before scaling, (b) after scaling

3.3.3 Incremental dynamic analysis (IDA)

Incremental dynamic analysis (IDA) was conducted to evaluate the response of the two prototype bridge structures with control columns. Although currently IDA is not widely used in practice due to high computational demand, the availability of increasingly powerful computers and algorithms makes it a promising and increasingly effective tool. IDA enables a thorough and systematic evaluation of the seismic performance of structures because it considers a wide range of ground motions with different frequency content and different intensity levels.

The development of the IDA method and details regarding the concepts are described in detail by Vamvatsikos and Cornell (2002). Accordingly, the following procedure was used to generate the IDA curves of the bridge models: (1) scaling each of the 40 selected GM records with an increment 0.1 g from zero to a value where numerical non-convergence of the dynamic analysis on the models occurred; (2) recording the maximum drift ratio at the top of the columns under the scaled records, while in the case of non-convergence the maximum drift ratio was set as infinity; and (3) plotting the relationship between the intensity measure (Sa (T1, 5%)) and the damage measure (maximum drift ratio) (He et al. 2016). Each point on each IDA curve is the result of a single dynamic analysis for the bridge model subjected to a single scaled GM. An average of 15 dynamic analyses, ranging from 0.1 to 1.5 times the GM scale factor, were performed to obtain a single IDA curve.

The analysis was conducted using the OpenSees framework, while the output was processed using the software MATLAB. A desktop computer with twelve logical processors was used to conduct the IDA of the two bridge models. It should be noted that the IDA method is analytically intensive, requiring many nonlinear analyses. The IDA curves of the Bridge A model with Column A control columns (Section 2.3) is shown in Figure 3.6. The IDA curves of

the Bridge B model with Column B control columns (Section 2.4) is shown in Figure 3.7. Each solid line in Figures 3.6 and 3.7 represents the relationship between Sa (T1, 5%) and the drift ratio demand on the columns for each GM record. The horizontal portion of each IDA curve represents the instability or non-convergence of analysis of the bridge model, i.e., at the corresponding Sa (T1, 5%) the structure may have collapsed.
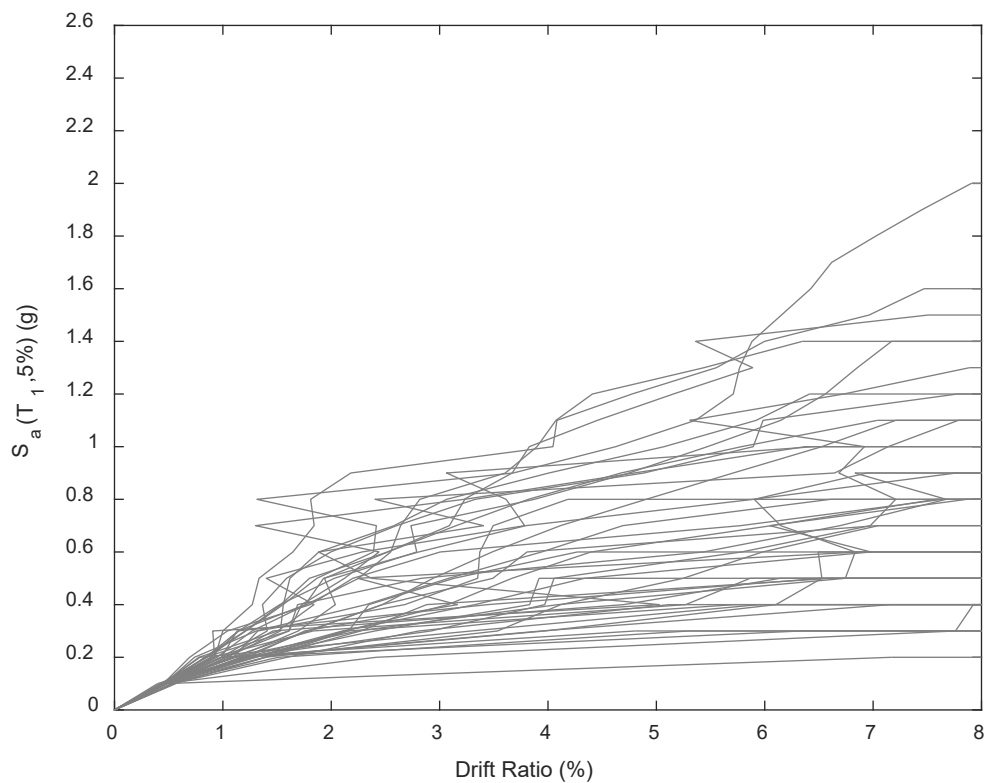

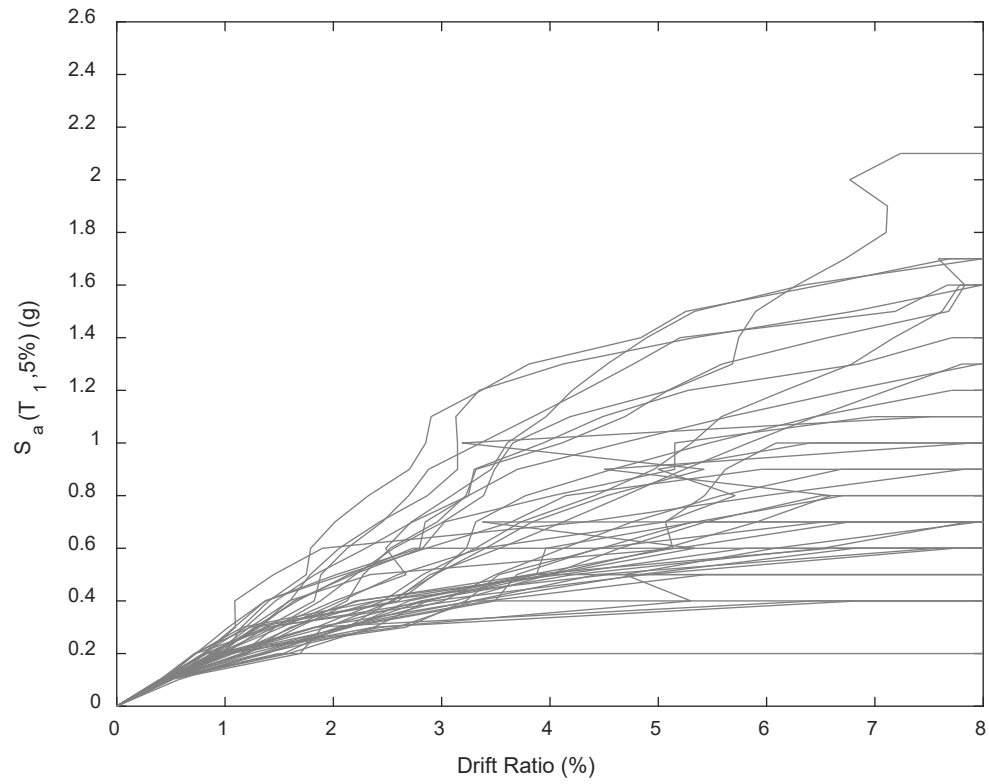**Figure 3.6** Bridge A: IDA curves of bridge model with Column A control columns using 40 GM records

Figure 3.7 Bridge B: IDA curves of bridge model with Column B control columns using 40 GM records

Chapter 4 Retrofit-Repair Optimization Methodology

4.1 Overview

     This section presents a framework developed to optimize the level of (pre-earthquake) retrofit of RC bridge columns that can be rapidly repaired (i.e., in a 3-day period) in the event of an earthquake. To do so, it is fundamental to define the RC bridge performance requirements in terms of strength and ductility. An extensive review of the literature on documented methods to repair RC bridge columns was previously conducted and summarized in a report by Sneed et al. (2019). The report findings address the question of what level of damage an RC bridge column can withstand and what level of damage is considered convenient to be repaired. Another important consideration is the level of seismic action that is expected in the site where the bridge is located.

     The first step of the retrofit-repair optimization methodology developed in this study was to use the IDA curves of the RC bridge with un-strengthened (control) columns to evaluate the bridge seismic performance, as shown in Chapter 3. Then, two performance requirements were set in terms of a drift ratio limit DR(L) and a spectral acceleration limit Sa(L). Finally, the RC bridge with retrofitted columns in different locations was evaluated using IDA with the aim of determining the best configuration (in this case, corresponding to the lowest number of retrofitted columns) for which the IDA curves did not exceed the prescribed limits.

4.2 Hazard and Damage States

     A descriptive formulation of damage states, where the severity of the damage is associated with a visible damage condition and mechanism, was proposed by Vosooghi and Saiidi (2010). The study, based on a comprehensive review of shake test data from 30 RC bridge columns, identified five damage states corresponding to five apparent levels of damage. The

damage states were defined as follows: DS-1: flexural cracks; DS-2 first spalling and shear cracks; DS-3: extensive cracks and spalling; DS-4: visible transverse and longitudinal bars; DS-5: imminent failure.

However, if the seismic event is so strong it results in column failure, where the contribution of the damaged column to the strength of the bridge structure is null, it is not possible to identify the damage state using the abovementioned scale. For this reason, the damage states scale proposed by Vosooghi and Saiidi (2010) was by expanded by Sneed et al. (2019) with a sixth state: DS-6: member failure. In addition, an additional damage state has been added to classify structural elements that, following a seismic event, exhibit damage that does not affect the performance: DS-0.

The literature search performed by Sneed et al. (2019) also showed that different repair methods were successfully implemented in many tests to restore, at least partially, the strength, stiffness, and ductility of RC columns up to DS-6. Table 4.1 shows the damage classification according to Sneed et al. (2019).

Table 4.1 Damage classification (Sneed et al. 2019)

Damage states	Damage classification	Damage description	Repair
DS-0	None	Barely visible damage	No repair
DS-1	Minor	Flexural cracks	Possible repair
DS-2	Minor/moderate	Minor spalling and shear cracks	Possible/minimum repair
DS-3	Moderate	Large cracks and spalling	Minimum repair
DS-4	Moderate/serious	Visible reinforcement	Moderate repair
DS-5	Serious	Core damage	Intensive repair
DS-6	Critical	Buckling or fracture of the reinforcement	Intensive repair/ replacement

This approach, although useful to use on site to evaluate the damage caused by a seismic event, is subjected to interpretation and not capable of defining unambiguous categories. Therefore, it is not suitable to be used in a numerical model.

Dutta and Mander (1999) defined five different damage states to categorize the severity of damage to an RC bridge element, ranging from almost no damage to collapse, where each state corresponds to a given drift limit. However, this scale is a function of the column design since the same drift ratio can cause different damage to a non-seismically designed column compared with a seismically designed column. Table 4.1 shows the damage for non-seismically and seismically designed RC columns.

Table 4.2 Drift limits according to Dutta and Mander (1999)

	Damage States	Non-Seismically Designed Drift Limit	Seismically Designed Drift Limit
S-1	First Yield	θ_y	θ_y
S-2	Cracking, Spalling	0.008	0.01
S-3	Loss of Anchorage	0.010	0.025
S-4	Incipient Pier Collapse	0.020	0.050
S-5	Pier Collapse	0.050	0.075

In the present study a drift ratio limit was chosen corresponding to a damage state defined as DS-5 by Sneed et al. (2019) and defined as S-4 by Dutta and Mander (1999). Therefore, the drift ratio limit was set as DR(L)=0.02 for Column A, and DR(L)=0.05 for Column B. It should be noted that while both Columns A and B were non-seismically detailed, a drift ratio limit of 0.05 was selected for Column B since the starter bars were fully anchored, and the compression buckling of the longitudinal bars could be prevented by the jacket. The approach herein is

considered conservative since the drift ratio limit values refer to the condition of the un-strengthened column, therefore neglecting the ductility increase caused by the retrofit. Alternatively, a second and less conservative approach is to calculate the drift ratio limit using the maximum horizontal displacement obtained during the cyclic analysis of retrofitted column (e.g., DR(L)=0.05 and DR(L)=0.06 for Column A and Column B, respectively). The second approach may be considered more appropriate when all bridge columns of a given bridge are retrofitted.

A spectral acceleration limit Sa(L)was chosen according to the AASHTO-2009 Guide Specification for LRFD Seismic Bridge Design for the city of Rolla, MO (USA), site class D, corresponding to a 1000-year earthquake return period on a 75-year bridge lifespan. The values of peak ground acceleration $PGA = 0.09$g, short-period spectral acceleration $S_s = 0.211$g, and 1-second spectral acceleration $S_1 = 0.074$g were provided by the United States Geological Survey (USGS) for the chosen location (USGS 2021). The city is in proximity of the New Madrid Seismic Zone. Figure 4.1 shows the design horizontal response spectrum, where the value of Sa(L)= 0.215g was chosen according to the value T1 determined for the prototype Bridge A and Bridge B with control columns (Chapter 3). Since a design response spectrum is constructed as a function of the probability that an earthquake will occur in a certain time range, a different value can be used as Sa(L) depending on the risk level that can be accepted. Figure 4.2 shows the drift ratio and spectral acceleration limitation applied in the case of Bridge A and Bridge B.
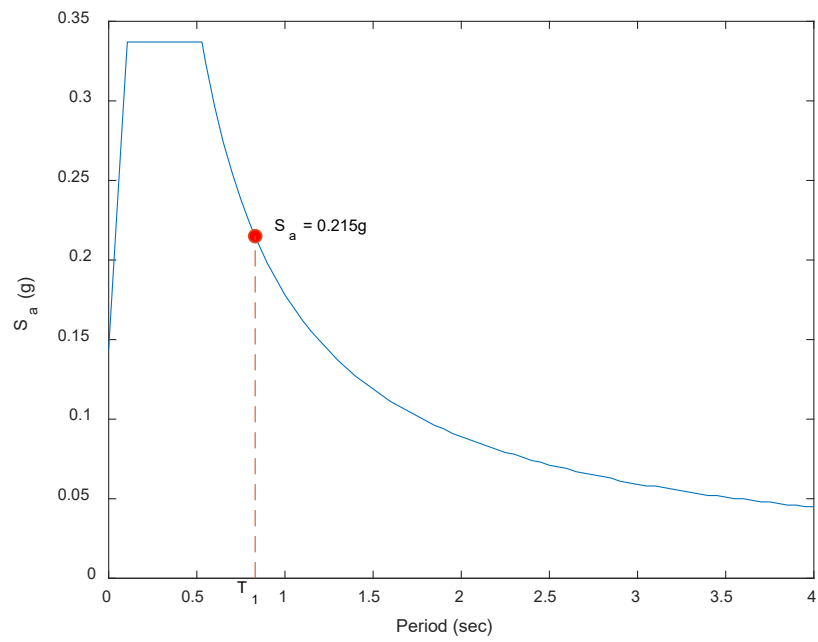
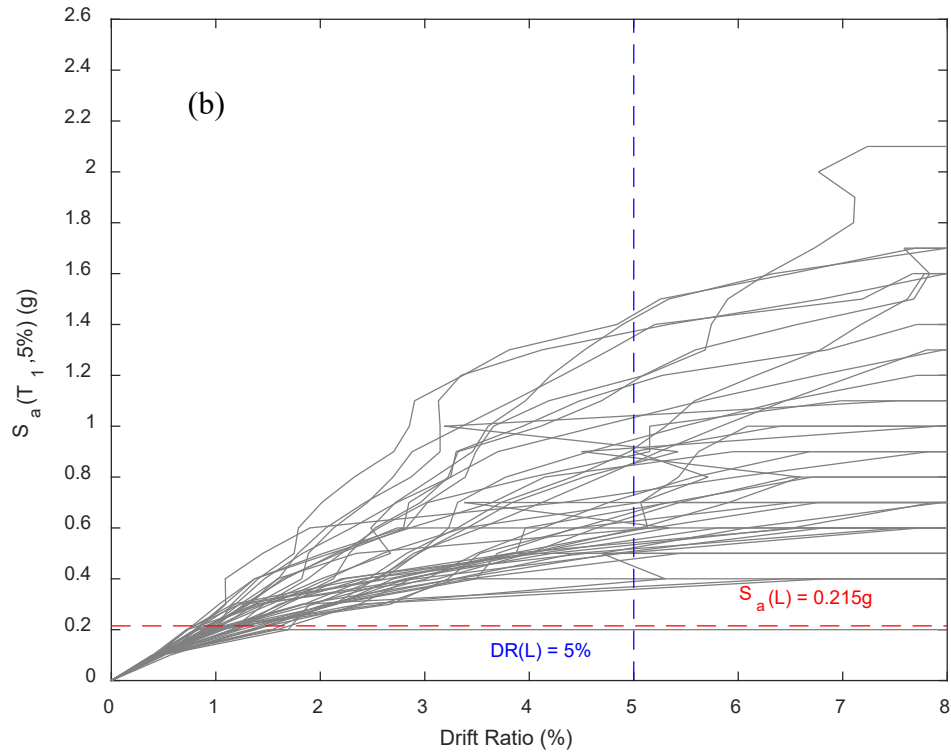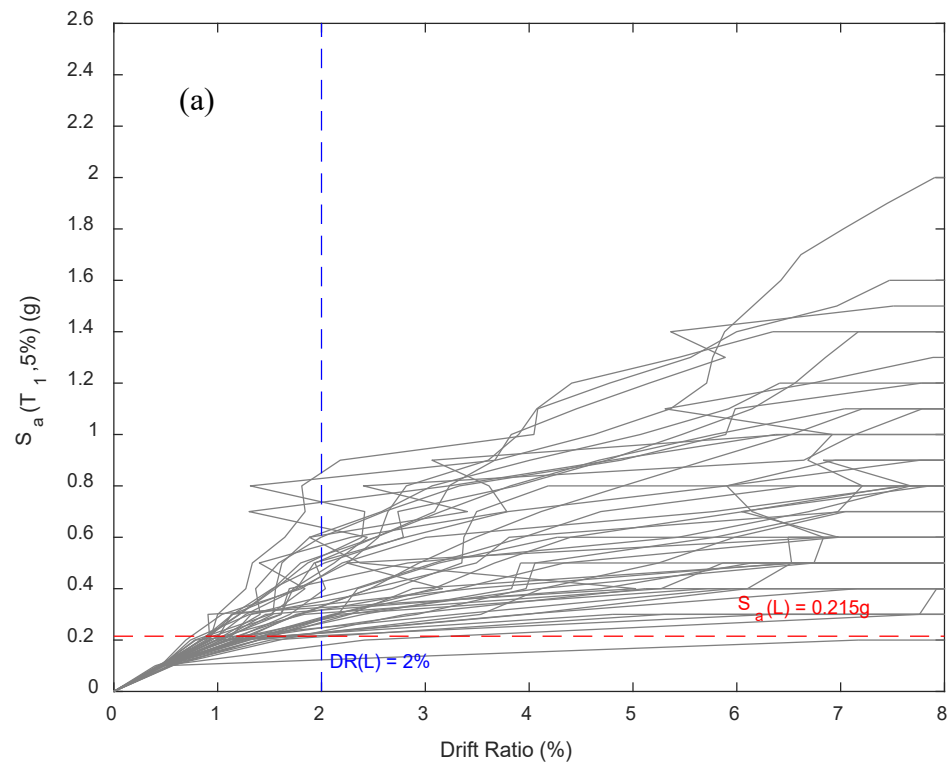**Figure 4.1** Horizontal response spectrum

Figure 4.2 Spectral acceleration limitation applied to: (a) Bridge A, (b) Bridge B

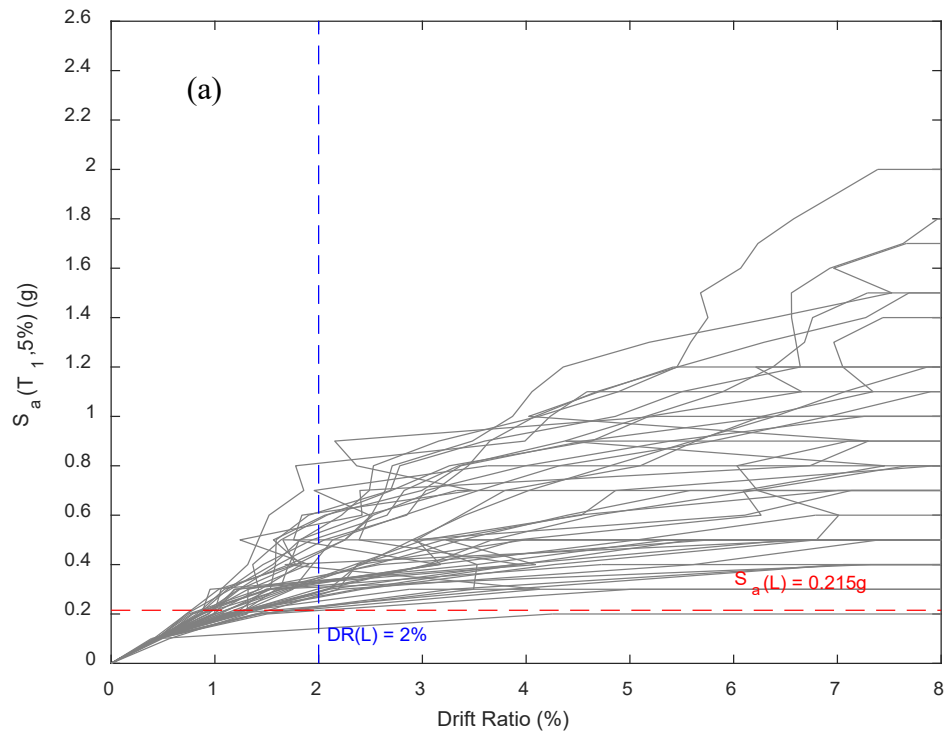## 4.3 Optimizing the Levels of Retrofit and Repair

4.3.1 Bridge A

IDA was conducted to evaluate the response of the prototype bridge structure with one or more retrofitted columns. The bridge structure models with different scenarios of retrofitted columns are referred as models Ret-1, Ret-12, Ret-13, Ret-14, Ret-123, and Ret-1234, where Ret indicates the model included one or more retrofitted column elements, and the numbers 1,2,3,4 identify the columns that were repaired in the model. Column numbers are defined in Figure 3.2. The other columns in each model were modeled as original columns. Results of models Ret-1, Ret-12 (or Ret-13 or Ret-14), Ret-123, and Ret-1234, which had 1, 2, 3, and 4 repaired columns, respectively, were used to study the influence of the number of retrofitted columns. Results of models Ret-12, Ret-13, and Ret-14, each with two repaired columns, were used to study the influence of retrofitted column location.

Since replacing control columns with retrofitted columns modifies the bridge fundamental frequency, the ground motion records were scaled, for each combination, accordingly. The fundamental frequency of each bridge model is summarized in Table 4.3.

The analysis was performed using OpenSees framework and the same procedure explained in Chapter 3. The analysis results, shown in Figure 4.3, were processed using the software MATLAB.

Table 4.3 Bridge A: Fundamental frequency of bridge structure model

		Mode 1 [longitudinal]	
	Bridge model	Frequency (Hz)	Period (sec)
Original (FHWA 1996)	Orig.	1.202	0.832
Control	Contr.	1.202	0.831
Retrofitted	Ret-1	1.232	0.824
	Ret-12	1.260	0.793
	Ret-13	1.262	0.792
	Ret-14	1.262	0.792
	Ret-123	1.290	0.775
	Ret-1234	1.317	0.759
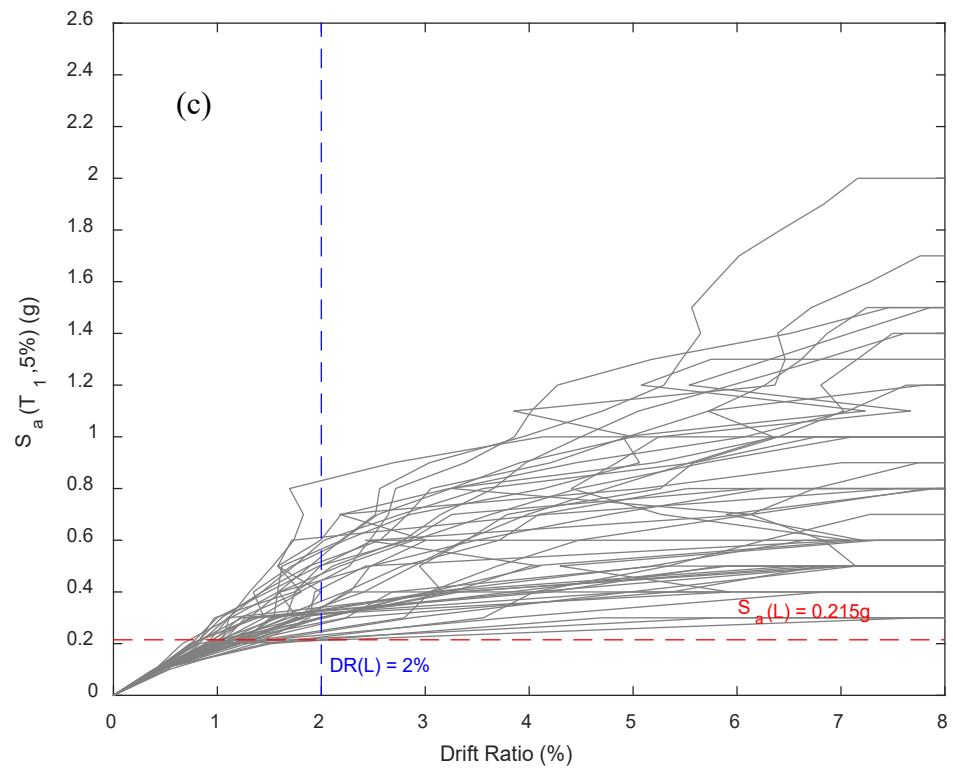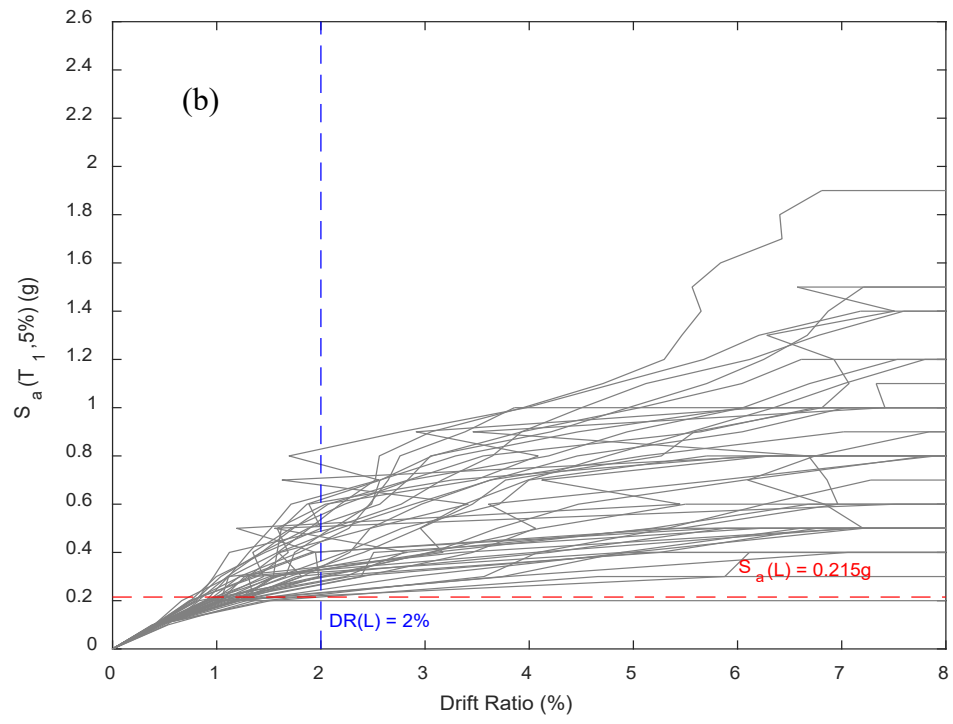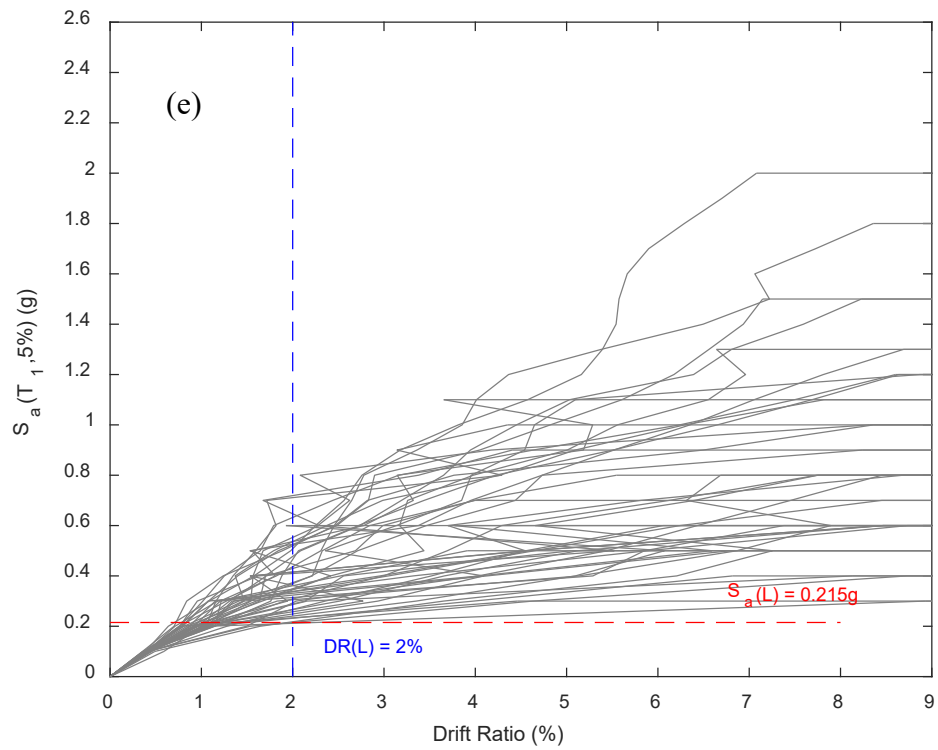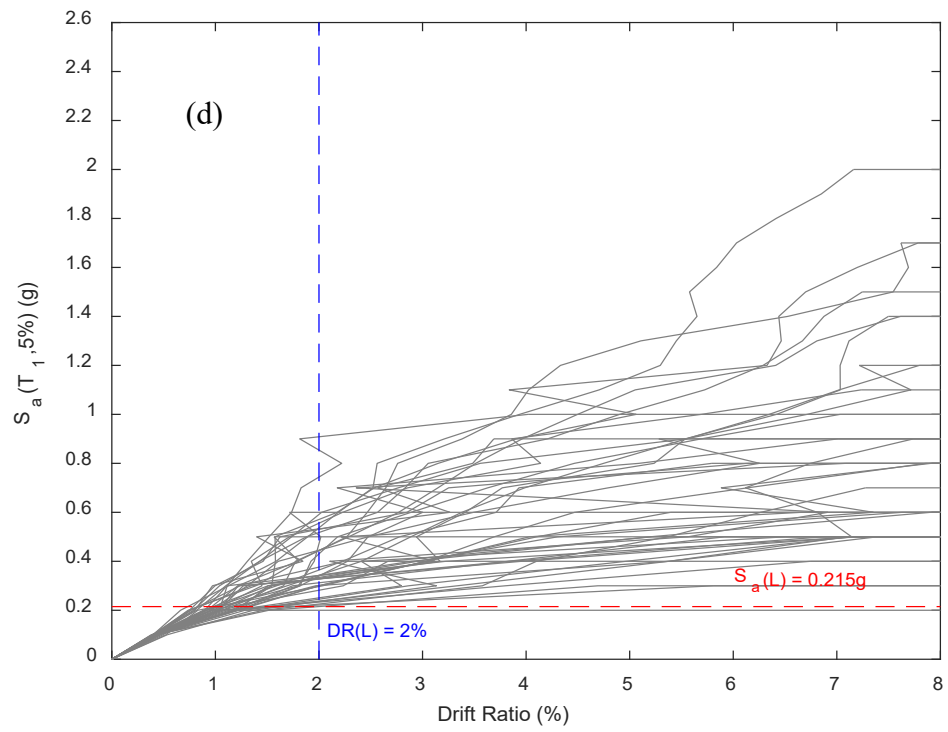
Figure 4.3 Bridge A: IDA curves of 40 GM records: (a) Ret-1; (b) Ret-12; (c) Ret-13; (d) Ret-14; (e) Ret-123; (f) Ret-1234**.**

4.3.2 Bridge B

Similar to Bridge A discussed in Section 4.3.1, IDA was conducted to evaluate the response of the prototype bridge structure Bridge B with one or more retrofitted control columns. The fundamental frequency of each bridge model is summarized in Table 4.4.

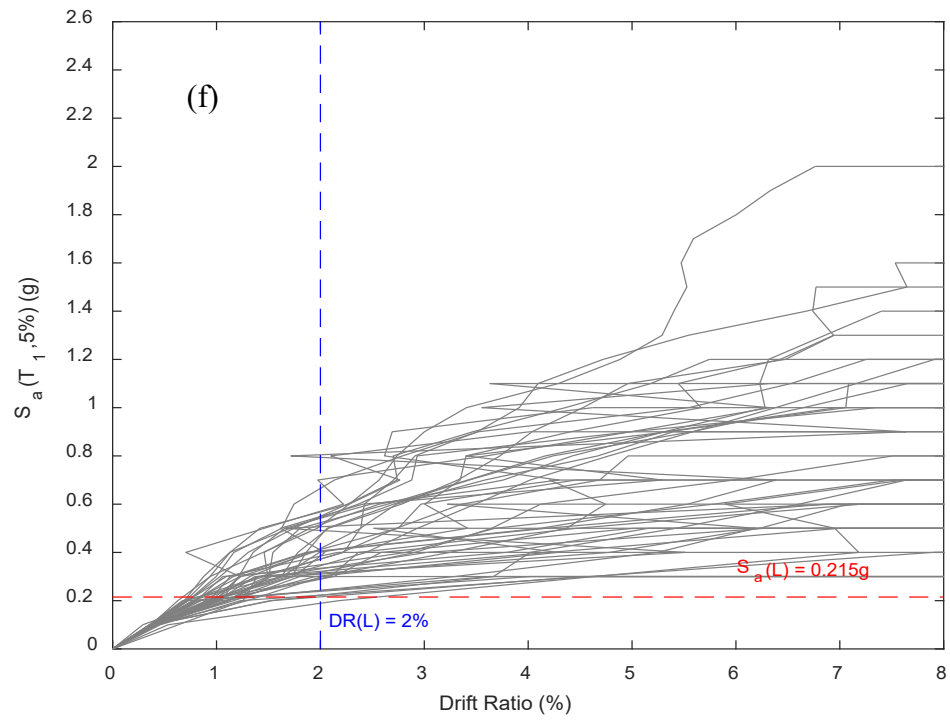Table 4.4 Bridge B: Fundamental frequency of bridge structure model

		Mode 1 [longitudinal]	
	Bridge model	Frequency (Hz)	Period (sec)
Original (FHWA 1996)	Orig.	1.202	0.832
Control	Contr.	1.202	0.832
Retrofitted	Ret-1	1.236	0.809
	Ret-12	1.268	0.788
	Ret-13	1.269	0.788
	Ret-14	1.269	0.788
	Ret-123	1.301	0.768
	Ret-1234	1.332	0.768

The analysis was performed using OpenSees framework and the same procedure explained in Chapter 3. The analysis results, shown in Figure 4.4, were processed using the software MATLAB.
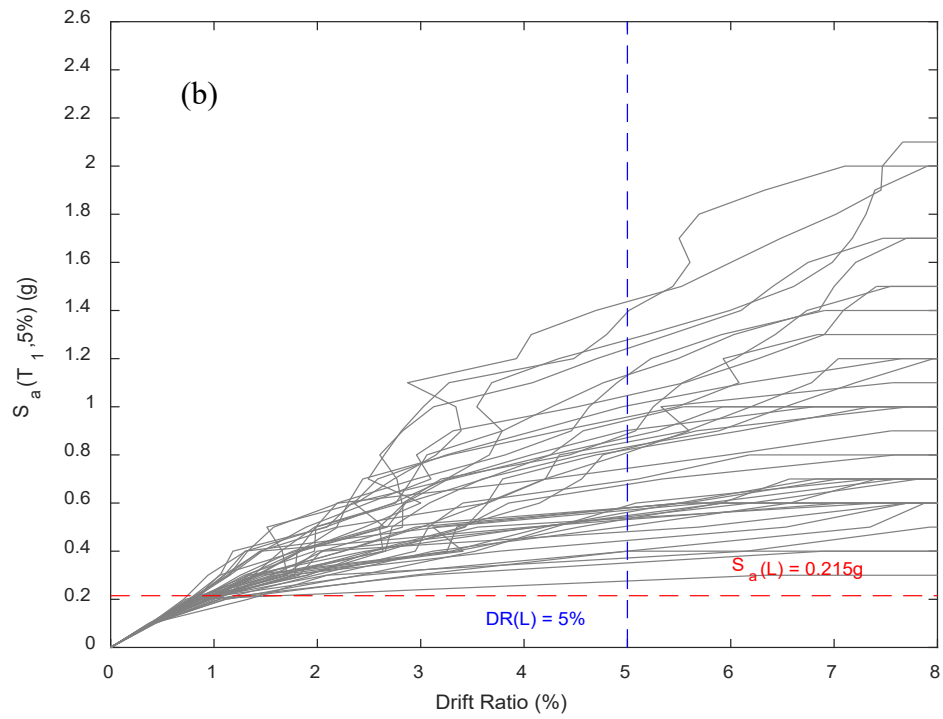
Figure 4.4 Bridge B: IDA curves of 40 GM records s: (a) Ret-1; (b) Ret-12; (c) Ret-13; (d) Ret-14; (e) Ret-123; (f) Ret-1234**.**

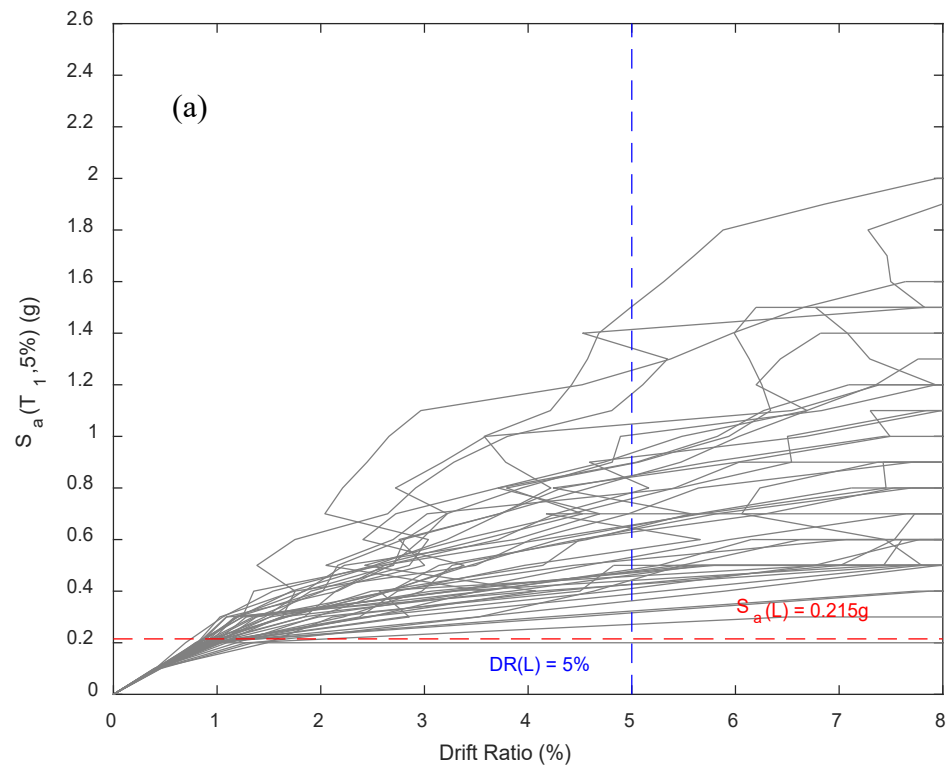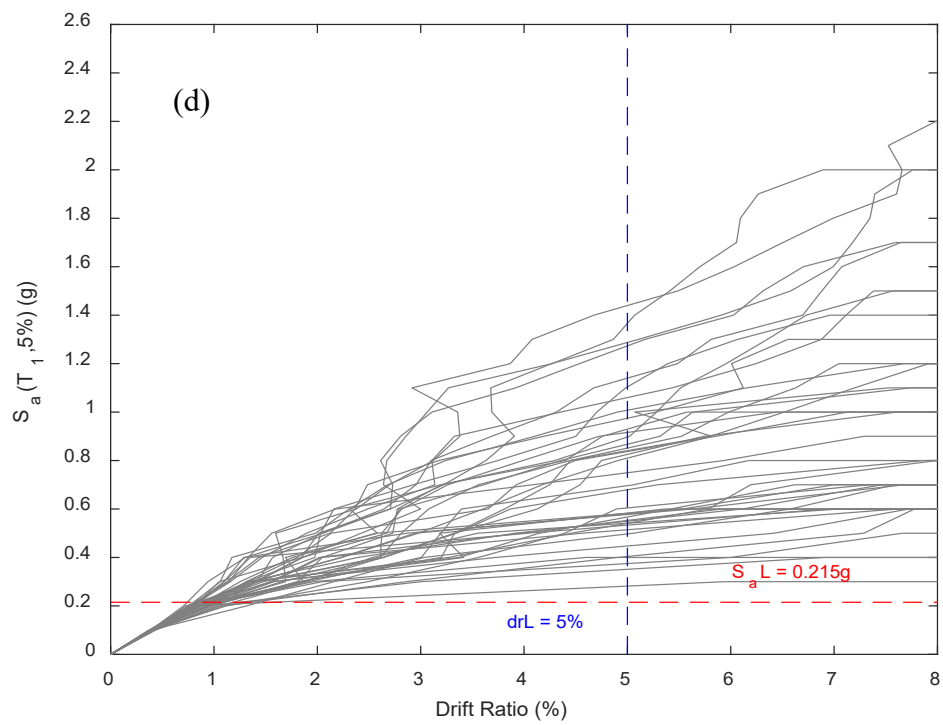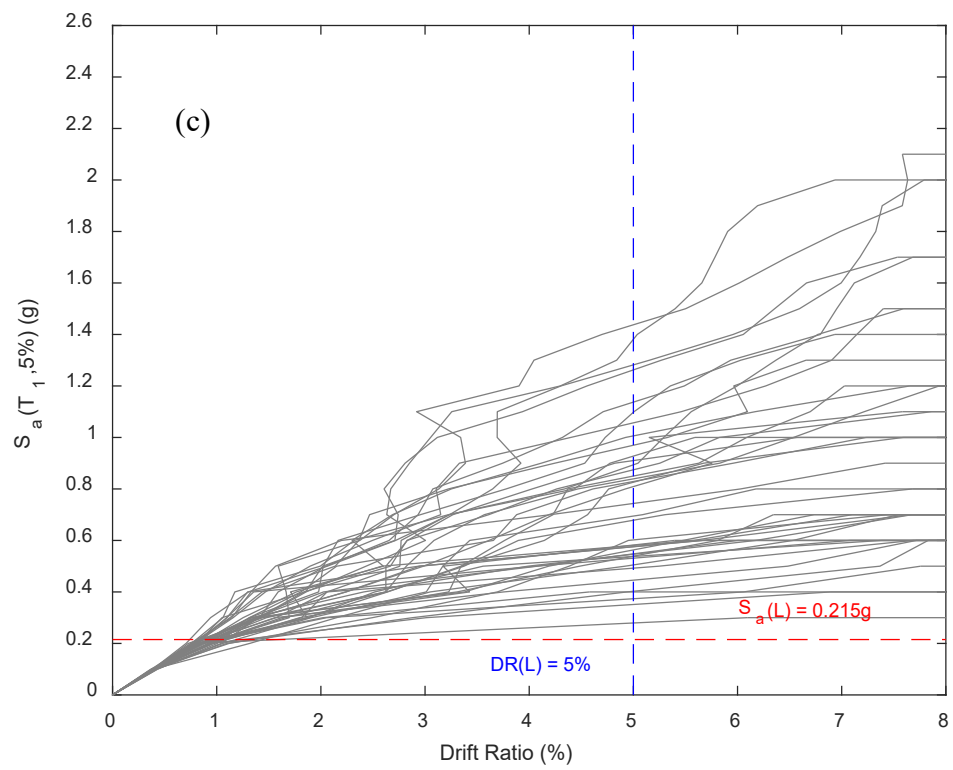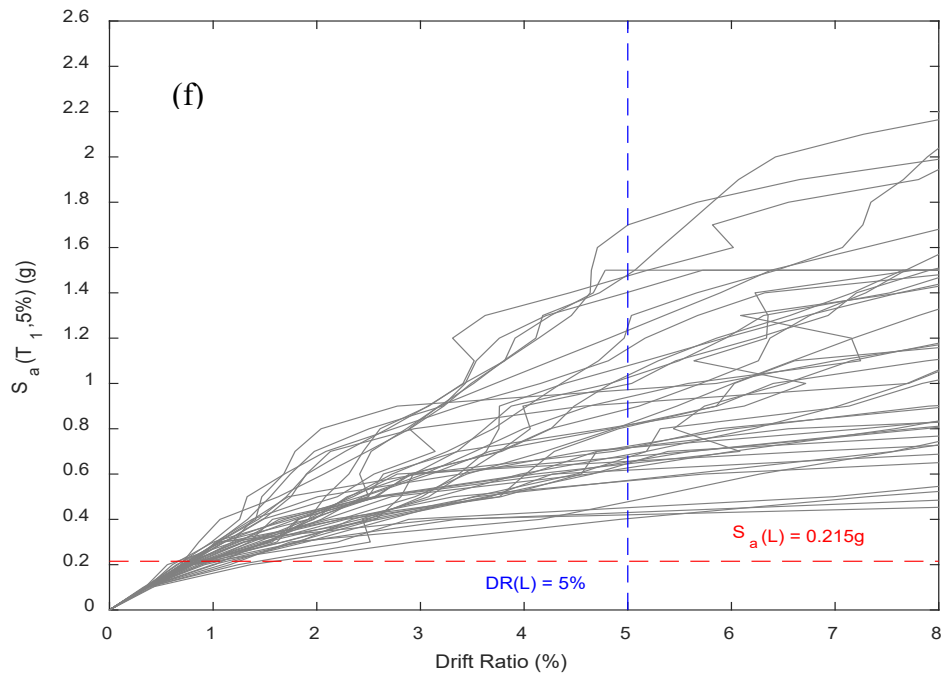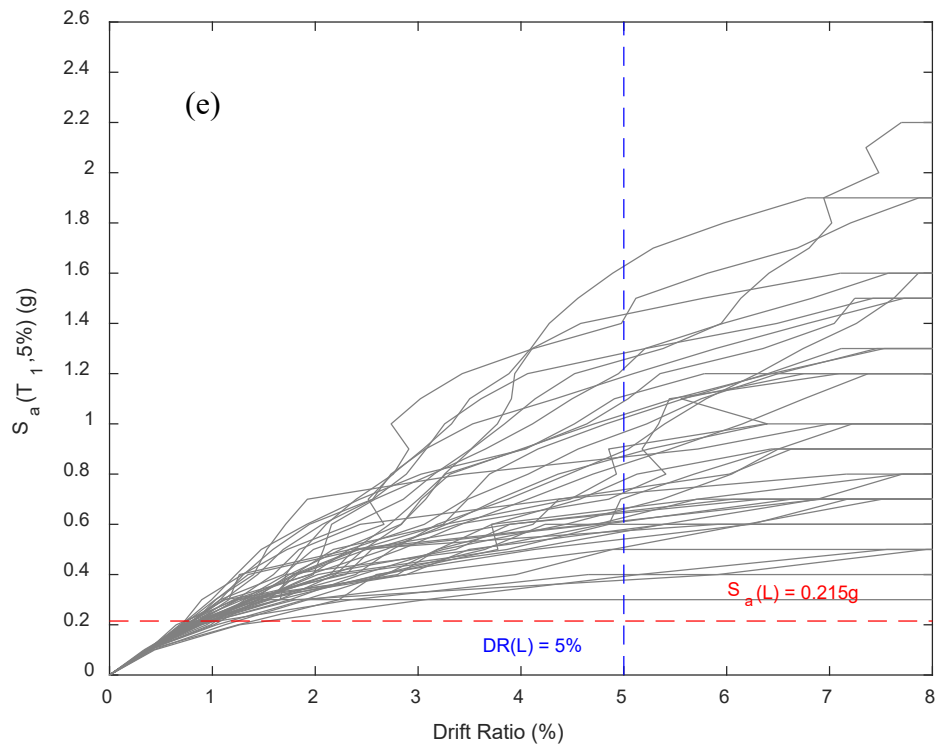4.4 Summary and Discussion

4.4.1 IDA results

Figures 4.3 and 4.4 show the IDA curves of the six bridge models with retrofitted

columns from Bridge A and Bridge B, respectively. The performance limits DR(L) and Sa(L)

discussed in Section 4.2 are indicated on each graph. The retrofit configuration is considered

successful if the corresponding IDA curves do not pass within the portion of the graph where the

drift ratio is larger than the drift ratio limit (i.e., drift ratio ≥ DR(L)) and the spectral acceleration

is smaller than the spectral acceleration limit (i.e., Sa (T1, 5%) ≤ Sa(L)).

Results presented in Figure 4.3 for Bridge A show that the retrofit method used for

Column A, although capable of significantly improving the bridge seismic performance, was

unable to prevent portions of certain IDA curves within the portion of the graph where the drift

ratio is larger than the drift ratio limit and the spectral acceleration is smaller than the spectral

acceleration limit. Models Ret-13, Ret-123, and Ret-1234, shown in Figures 4.3c, e, and f,

respectively, had curves that exceeded drift ratio limit (2%) at spectral accelerations lower than

the limit (0.215g), whereas Models Ret-1, Ret-12, and Ret-14, shown in Figures 4.3a, b, and d,

respectively, had curves that indicated collapse at values of spectral acceleration lower than the

limit.

Since the retrofit method was found to be unsuccessful for all configurations considered,

an alternative retrofit design was explored. In this case, the retrofit of Column A was increased

by adding an additional layer of the GFRP jacket configuration shown in Figure 2.6. The

numerical cyclic behavior of the improved retrofitted column is shown in Figure 4.5, which

shows the enhancement due to the additional jacket layer. Table 4.5 summarizes the bridge

fundamental frequency for Bridge A with three improved retrofitted columns in positions 1,2,3,

named Improved Ret-123. Figure 4.6 presents the corresponding IDA curves of the model Improved Ret-123, which indicate that the improved retrofit design proved to be capable of avoiding bridge collapse under the limits proposed in Section 4.2. In this way, the retrofit design could be reverse engineered to meet the performance requirements.
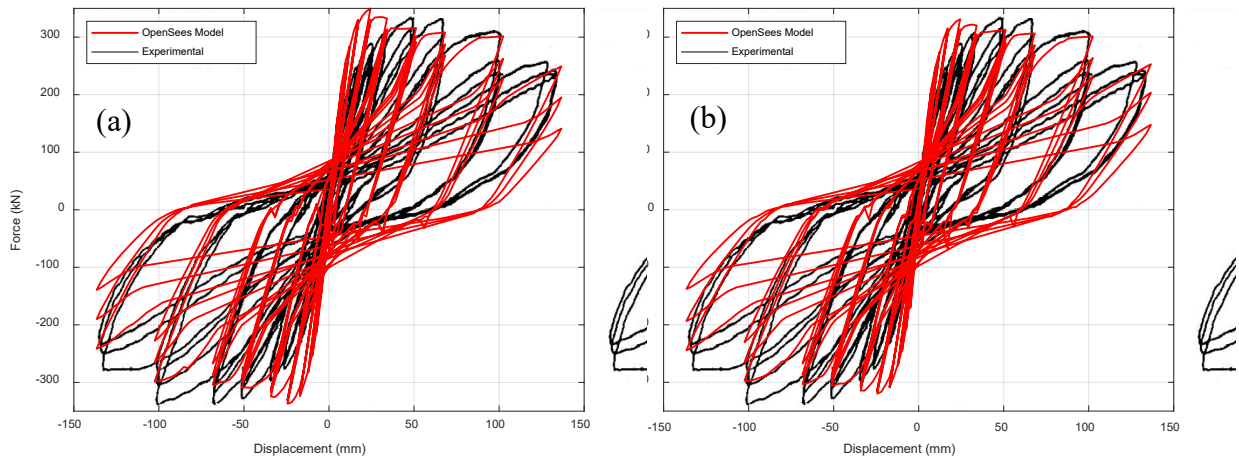
Figure 4.5 Column A: numerical and experimental cyclic behavior of (a) improved retrofitted column, and (b) retrofitted column
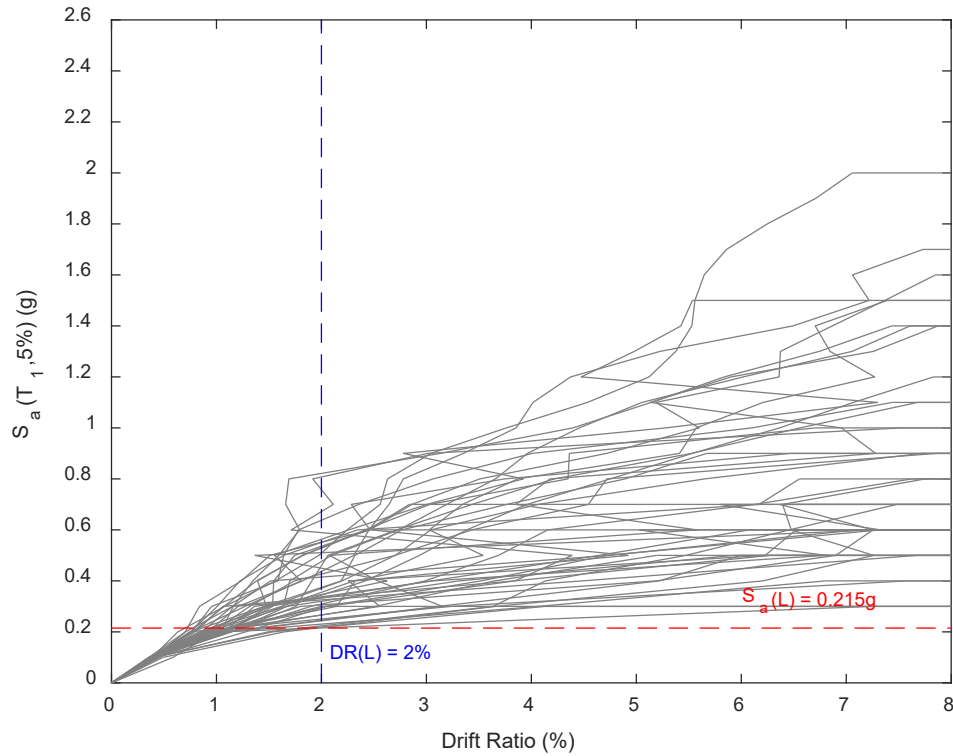
Figure 4.6 Experimental Test A: IDA curves of 40 GM records: Improved Ret-123

Table 4.5 Bridge A: Fundamental frequency of improved bridge structure model

		Mode 1 [longitudinal]	
	Bridge model	Frequency (Hz)	Period (sec)
Improved	R-123	1.292	0.773

Results presented in Figure 4.4 for Bridge B proved that the retrofit method implemented to strengthen Column B was capable to avoid collapse of the RC bridge under the limits proposed in Section 4.2. The IDA curves of models Ret-12, Ret-13, Ret-14, Ret-123, and Ret-1234, with two or more retrofitted columns, were within the prescribed limits (see Figures 4.4b-f). On the other hand, model Ret-1, with one retrofitted column, had curves that indicated collapse at values of spectral acceleration less than the limit (see Figure 4.4a). Accordingly, for

48

Bridge B, two retrofitted columns, in any locations, were found to be the optimized level of pre-earthquake retrofit in order to have a reparable bridge after the expected seismic event. A further increase in the effort of retrofitting, although capable of improving the overall seismic endurance of the RC bridge, does not affect the bridge capacity of being repaired and likely leads to an increase of cost, especially if no seismic event effects the structure.

4.4.2 Approach limitations

The IDA method aims to study the structure behavior transitioning from the elastic to the post-yield phase. The first mode spectral acceleration Sa (T1, 5%), gives only an indication of the bridge elastic first mode response. Therefore, the conceptual framework of IDA analysis loses validity after reaching the post-yielding phase of the response (Kunnath and Kalkan 2005).

In this work, the earthquake scaling was performed taking into consideration only the fundamental period, which is only an approximation of the physical domain. The scaling procedure especially increases those earthquakes that have a weak frequency content corresponding to the structure fundamental frequency and penalizes seismic records that show strong frequency content corresponding to the structure fundamental frequency. An example is provided in Figure 4.7, which shows the pseudo spectral acceleration corresponding to Earthquake Set 7, Record Number 14 from Table 3.1, where the range of the fundamental periods of the bridges modeled in the present study fall within the spectral acceleration local minimum. This seismic record is the one that led to discard the retrofit configurations analyzed in Figure 4.3d and e for Bridge A and Figure 4.4a for Bridge B.
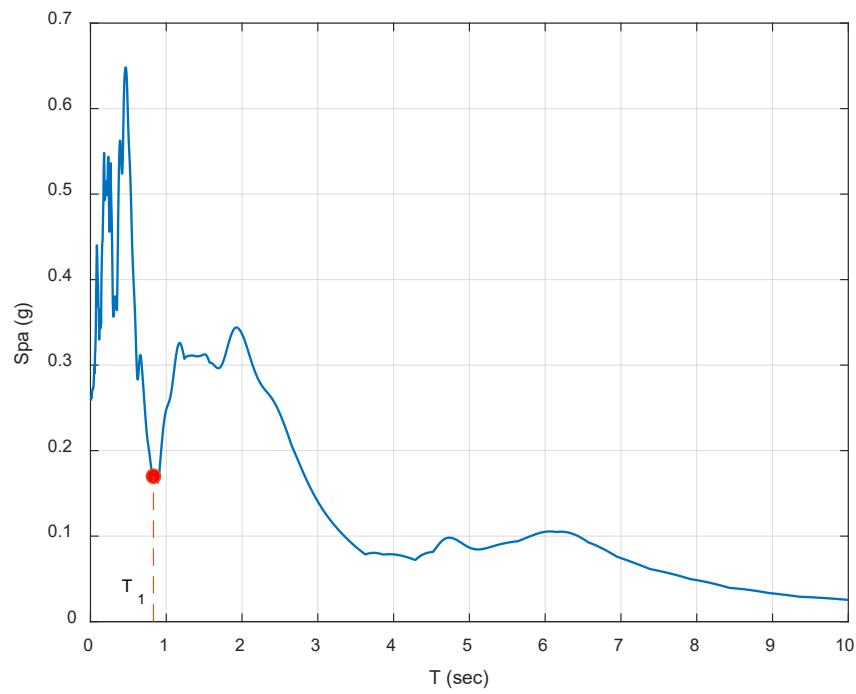
Figure 4.7 Superstition Hills-02 1987 El Centro Imp. Co. Cent Elastic Pseudo Spectral Acceleration (5% damping)

Chapter 5 Conclusion

The IDA method enables a thorough and comprehensive evaluation of the seismic

performance of a structure considering different sources of variability, and using ground motion

records with different frequency contents and for different levels of seismic intensity.

The application of the IDA method is analytically intensive, requiring many nonlinear analyses,

and is currently not commonly used in design practice. However, advancement in new

algorithms and new hardware help reduce the computational time, making the method more

feasible.

In this study, more than 8000 time-history analyses were performed to assess the seismic

performance of an RC bridge built with two different column designs, with the purpose of

optimizing the level of (pre-earthquake) retrofit and (post-earthquake) repair.

The methodology adopted in this study to simulate the response of the bridge columns

and bridge systems was similar to that used in Phase I of this research and was based on previous

work by He et al. (2016). In the present work reported herein, i.e., Phase II, the method was

extended to columns with different retrofit conditions. The control and retrofitted numerical

models presented in this report were developed in OpenSees and validated against experimental

data. The three-span RC prototype bridge was also modeled in OpenSees and validated using a

design example reported in the literature. The IDA was conducted on the prototype bridge model

that incorporated the developed column models employing 40 ground motion (GM) records,

which were selected and scaled according to the target design response spectrum.

Results of this work showed the cyclic response of control RC columns can be

reproduced numerically using a classical approach with negligible discrepancy in terms of initial

stiffness, base shear capacity, strength degradation, and stiffness degradation. Although similar,

modeling the response of retrofitted RC columns required a thorough evaluation of the retrofit design in order to accurately simulate the response.

Regarding the bridge system-level response, although the IDA results showed that retrofitting the column members increases the bridge seismic performance, the increase is not always sufficient to ensure that damage suffered by the bridge columns can be successfully repaired. This point was illustrated by evaluating the response of the three-span RC prototype bridge with control and/or retrofitted columns subjected to the selected GM records. Considering the performance requirements employed (in terms of drift ratio and spectral acceleration limits), IDA results of Bridge A with retrofitted columns showed that the retrofit method was not successful in meeting the performance requirements, even if all columns of the bridge were retrofitted. Therefore, an approach was presented to design a column retrofit that could meet the performance requirements. In contrast, IDA results of Bridge B showed that a minimum of two retrofitted columns (of the four columns in the bridge) in any location would be adequate to provide repair to a bridge after the expected seismic event. This knowledge could be used to optimize the retrofit and reduce the initial cost.

References

AASHTO (1995). "Standard Specifications for Highway Bridges, 15th ed". *American Association of Highway Transportation Officials, Washington, D.C.*

AASHTO, 2009, Guide Specifications for LRFD Seismic Bridge Design. Washington, DC: American Association of State Highway and Transportation Officials

Bradley, B., Dhakal, R., and Mander, J. B. (2006). Dependency of Building Fragility to source mechanisms of records selected for Incremental Dynamic Analysis.

Chai, Y.H., Priestley, M.J., and Seible, F. (1991). "Seismic retrofit of bridge columns by steel jacketing". *Transportation Research Record*.

Dutta, A., and Mander, J. B. (1999). "Seismic fragility analysis of highway bridges." *Proc., Center-to-Center Project Workshop on Earthquake Engineering in Transportation Systems*, Tokyo, Japan.

FHWA (1996). "Seismic design of bridges—Design example no. 4: Three-span continuous CIP concrete bridge." *Publication No. FHWA-SA-97-009*.

Fraioli, G., and Sneed, L. H. (2021). "Performance Investigation of Earthquake Damaged Reinforced Concrete Bridges with Repaired Columns" *(No. 25-1121-0005-136-2). Missouri University of Science and Technology.*

French CW, Thorp GA, Tsai WJ. Epoxy repair techniques for moderate earthquake damage. ACI Struct J 1990;87(4):416–24.

Fukuyama, K., Higashibata, Y., and Miyauchi, Y. (2000). "Studies on repair and strengthening methods of damaged reinforced concrete columns." *Cement & Conc. Compos.,* 22: 81-88.

He, R., Yang, Y., and Sneed, L. H. (2016). "Post-repair seismic assessment of RC bridges damaged with fractured column bars–A numerical approach." *Engineering Structures*, *112*, 100-113.

Kunnath, S. K., and Kalkan, E. (2005). IDA capacity curves: the need for alternative intensity factors. In *Structures Congress 2005: Metropolis and Beyond* (pp. 1-9).

Lehman, D.E., Gookin, S.E., Nacamuli, A.M., and Moehle, J. P. (2001). "Repair of earthquake-damaged bridge columns". *ACI Structural Journal,* 98: 233-242.

Mander, J. B., Priestley, M. J., and Park, R. (1988). "Theoretical stress-strain model for confined concrete." *Journal of Structural Engineering*, *114*(8), 1804-1826.

Mazzoni, S., McKenna, F., Scott, M. H., and Fenves, G. L. (2006)." OpenSees command language manual". *Pacific Earthquake Engineering Research (PEER) Center*, *264*.

McKenna F, Fenves GL, Scott MH, Jeremic B. Open system for earthquake engineering simulation (OpenSees). Pacific Earthquake Engineering Research Center. Berkeley (CA): University of California; 2000.

Paulay, T., and Priestley, M. N. (1992). "Seismic design of reinforced concrete and masonry buildings". *New York: Wiley.*

PEER, Pacific Earthquake Engineering Research Center. http://peer.berkeley.edu/peer_ground_motion_database [Accessed 12.20.21].

Scott BD, Park R, and Priestley MJN (1982). "Stress-strain behavior of concrete confined by overlapping hoops at low and high strain rates". *ACI Journal Proceedings*; 79 (1):13–27.

Shao, Y., Aval, S., and Mirmiran, A. (2005). "Fiber-element model for cyclic analysis of concrete-filled fiber reinforced polymer tubes." *Journal of Structural Engineering*, *131*(2), 292-303.

Sneed, L. H., Fraioli, G., and Alabdulhady, M. (2019). "Guide for the Selection of Rapid Repair Systems for Earthquake-Damaged Reinforced Concrete Bridge Columns" *(No. 25-1121-0005-136-1). Missouri University of Science and Technology.*

USGS, United States Geological Survey. https://earthquake.usgs.gov/ws/designmaps/aashto-2009.html [Accessed 12.15.2021]

Vamvatsikos, D., and Cornell, C. A. (2002). "Incremental dynamic analysis". *Earthquake Engineering & Structural Dynamics*, 31(3), 491-514.

Vosooghi, A. and Saiidi, M. S. (2010). "Seismic damage states and response parameters for bridge columns." *Special Publication*, *271*, 29-46.

Vosooghi, A., and Saiidi, M.S. (2009). "Rapid repair of high-shear earthquake-damaged RC bridge columns." *Proc., 25th US-Japan Bridge Engineering Workshop*, Tsukuba, Japan.

Xiao, Y., and Ma, R. (1997). "Seismic retrofit of RC circular columns using prefabricated composite jacketing." *Journal of Structural Engineering*, *123*(10), 1357-1364.

Xiao, Y., and Ma, R. (1997). "Seismic retrofit of RC circular columns using prefabricated composite jacketing". *Journal of Structural Engineering-asce*, 123, 1357-1364.

Zhao, J., and Sritharan, S. (2007). "Modeling of strain penetration effects in fiber-based analysis of reinforced concrete structures". *ACI Materials Journal*, *104*(2), 133.

Zhu, Z., Ahmad, I., and Mirmiran, A. (2006). "Fiber element modeling for seismic performance of bridge columns made of concrete-filled FRP tubes." *Engineering Structures*, *28*(14), 2023-2035.